Die approbierte Originalversion dieser Diplom-/Masterarbeit ist in der Hauptbibliothek der Technischen Universität Wien aufgestellt und zugänglich.
http://www.ub.tuwien.ac.at

The approved original version of this diploma or master thesis is available at the main library of the Vienna University of Technology.
http://www.ub.tuwien.ac.at/eng

TECHNISCHE UNIVERSITÄT WIEN
Vienna University of Technology

DIPLOMARBEIT

Adaptation of an Elasto-Plasto-Damage Model from Abaqus/Standard to Abaqus/Explicit and its Application to Laminated FRP Composites

ausgeführt zum Zwecke der Erlangung des akademischen Grades eines Diplom-Ingenieurs unter Leitung von

Associate Prof. Dipl.-Ing. Dr.techn. Heinz Pettermann
Finite Elemente Methoden
E317
Institut für Leichtbau und Struktur-Biomechanik

eingereicht an der Technischen Universität Wien
Fakultät für Maschinenwesen und Betriebswissenschaften

von

Broger Johannes
e0726068
Im Kirchholz 12 6845 Hohenems

Wien, am 25.2.2014 Broger Johannes

Contents

Acknowledgement

This work was carried out as a master thesis at the Institute of Lightweight Design and Structural Biomechanics (ILSB) at the Vienna University of Technology, hosting a node of the Polymer Competence Center Leoben (PCCL). The funding from the PCCL within the framework of the COMET-K1-program of the Austrian Ministry of Traffic, Innovation, and Technology and the State Government of Styria and Upper Austria is greatly acknowledged.

Thanks to all members of the ILSB to for creating the nice and supportive working environment I found. Special thanks to my thesis advisor, Heinz Pettermann.

Thanks to my family for their support during my time in Vienna.

Abstract

In the present thesis the constitutive behaviour of unidirectional fibre reinforced polymer composites is investigated. The Finite Element Method (FEM) is ideally suited for the simulation of structures with such a non-linear material behaviour. It is mostly used in an implicit formulation. This implicit form has some severe drawbacks in some applications, as for example convergence problems can occur when highly non-linear behaviour is to be simulated, possibly involving contact definitions. Another disadvantage is the high amount of working storage needed when big models are to be simulated and a possibly long calculation time. To circumvent some of these problems, an existing constitutive law, the elasto-plasto-damage-model (EPD) by Thomas Flatscher (2010, VDI Verlag, Duesseldorf) is adapted to be used in conjunction with the explicit FEM in quasi-static simulations. Because the original implementation was done for the use with Abaqus/Standard, it is obvious to adapt it to Abaqus/Explicit. To this end an interface is developed which incorporates the given EPD-model from Flatscher and makes the necessary adjustments arising from the explicit FEM.

The implemented model is verified by comparing its predictions to the original model. The differences in the predictions are nearly vanishing and can be explained by round off errors and the changed integration method. To investigate the characteristic in terms of numerical efficiency, stability and its hardware requirements, some representative quasi-static simulations are conducted. A three point bending specimen, made out of two layers of ply, is investigated to show some key features of the EPD-model. The main part of the applications is subjected to open hole tension tests with various layups. These simulations combine the EPD-model to describe the constitutive response of the plies with cohesive elements to describe the interface between the plies. With this approach it is possible to model and efficiently simulate every single ply in the laminate as well as the interfaces. The results of the simulations are compared to experimentally obtained results from [Fla12] (2012, Composite Science and Technology, 72, p. 1090-1095, Elsevier). They are generally in good agreement, although some inconsistencies exist. Finally an unit cell of a braided composite from the Ph.D.-thesis

of Jakob Gager (2013, PhD thesis, ILSB, Vienna Univerity of Technology) is simulated to investigate the performance of the explicit integration scheme. The results could be reproduced, but no clear advantage of the explicit over the implicit FEM solver could be found.

Concluding it can be said, the combination of the EDP-model to describe the constitutive response of the plies with cohesive elements to describe the interface between the plies is very promising. It is possible to investigate every ply on its own including the interfaces in between. The explicit FEM is, due to its robustness, able to advantageously execute these highly non-linear simulations. The explicit simulations are found to by numerical efficient, depending on the specimens geometry, and the requirements on computer hardware are very small.

Kurzfassung

In der vorliegenden Arbeit wurde das Materialverhalten von unidirektional langfaserverstärkten Polymer-Verbundwerkstoffen untersucht. Die Methode der Finiten Elemente (FEM) eignet sich hervorragend zur Beschreibung und Simulation solcher Strukturen. Die FEM wird meist in einer impliziten Formulierung verwendet. Diese implizite Formulierung hat jedoch in gewissen Anwendungen den Nachteil, dass Konvergenzprobleme bei stark nichtlinearen Problemstellung, welche möglicherweise auch Kontaktbedingungen enthalten, auftreten können. Ein weiterer Nachteil ist die hohe Anforderung an die Größe des Arbeitsspeichers bei großen Modellen, sowie eine möglicherweise sehr lange Rechenzeit. Um einige dieser Probleme zu umgehen, wurde ein bestehendes Materialmodell, das Elasto-Plasto-Schädigungsmodell (EPD) von Thomas Flatscher (2010, VDI Verlag, Duesseldorf), angepasst, um es in Kombination mit der expliziten FEM verwenden zu können. Da die ursprüngliche Formulierung zur Verwendung mit Abaqus/Standard entwickelt wurde, liegt es Nahe diese Formulierung zur Verwendung mit Abaqus/Explicit anzupassen. Zu diesen Zweck wurde eine Subroutine entwickelt, welches das vorhanden Modell von Thomas Flatscher enthält, und einige

notwendige Anpassungen vornimmt, welche sich aus den Anforderungen der expliziten FEM ergeben.
Das implementierte Modell wurde verifiziert, sprich mit dem ursprünglichen Modell verglichen. Die Abweichungen sind verschwindend und lassen sich auf Rundungsfehler sowie die veränderte Integrationsmethode zurückführen. Um die Eigenschaften bezüglich numerischer Effizienz und Stabilität, sowie der Hardware-Anforderungen zu untersuchen wurden einige repräsentative Probleme simuliert. Ein Drei-Punkt-Biegebalken aus zwei Einzellagen wurde untersucht um einige Eigenschaften des EPD-Modells aufzuzeigen. Im Hauptteil des Anwendungsteils wurden Simulationen zu einer Lochplattengeometrie mit unterschiedlichem Lagenaufbau durchgeführt. In diesen Simulationen wurden die Möglichkeiten des EPD-Modells zur Beschreibung des Verhaltens der Einzellagen mit sogenannten Kohäsiv-Elementen welche das Interface beschreiben, kombiniert. Dadurch kann jede Einzellage, wie auch jedes Interface, sprich deren Einzelverhalten im Verbund untersucht werden. Diese Ergebnisse wurden mit experimentellen Ergebnissen aus der Literatur (2012, Composite Science and Technology, 72, p. 1090-1095, Elsevier) verglichen. Die Übereinstimmungen zwischen Simulation und Experiment ist in weiten Teilen sehr gut, obwohl teilweise Unterschiede feststellbar sind. Abschließend wurde eine Einheitszelle aus der Dissertation von Jakob Gager (2013, PhD thesis, ILSB, Vienna Univerity of Technology) betrachten, um weitere Vorteile der expliziten Zeitintegration zu ergründen. Die Ergebnisse konnten reproduziert werden, jedoch wurden keine gravierenden Vorteile hinsichtlich der Effizienz und Genauigkeit gefunden.

Abschließend kann angemerkt werden, dass die Kombination des EPD-Modells mit einer Formulierung für die Beschreibung der Interfaces in Kombination mit der expliziten FEM einige Vorteile aufweist. Es ist möglich das Laminat mit all seine Einzellagen zu simulieren und auszuwerten, auch Delaminationserscheinungen können erfasst werden. Die explizite FEM kann ihren Vorteil, ihre Robustheit, in diesen stark nichtlinearen Simulationen voll ausspielen. Die Rechenzeit ist abhängig von der Geometrie des Bauteils sehr kurz, und die Anforderungen an den Arbeitsspeicher sind sehr klein.

Notations

Abbreviations

FEM	Finite Element Method
FRP	fiber reinforced polymer
UD	unidirectional

Subscripts

x, y, z	laminate coordinates
$1, 2, 3$	ply coordinates
ξ, η, ζ	braid coordinates

Superscripts

Superscript on the right side of variables refer to the material state.

(0)	refers to the virgin ply material
(el)	refers to elastic strains
(pl)	refers to plastic strains
(t)	refers to tension
(c)	refers to compression
(f)	refers to fiber
(m)	refers to matrix
(i)	refers to time increment i

Coordinate systems

For fibre reinforced laminates consisting of a number of stacked plies it is common to define a local ply coordinate system, $1, 2, 3$, for each individual ply. These local coordinate system define the fibre direction ,1, the in plane transverse direction ,2, and the out of plane transverse direction ,3. For each ply the fibre orientation is given by the angle ψ, referring to the laminate coordinate system, x, y, z, see figure 1. The coordinates $(1, 2)$ and (x, y) denote the in plane directions.

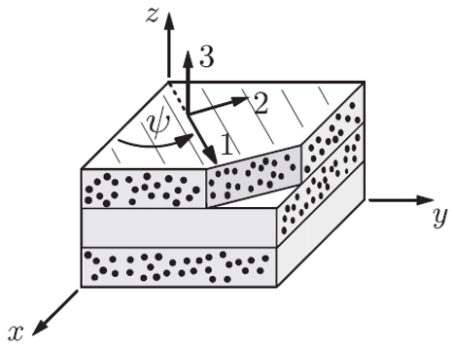

Figure 1: Sketch of a laminate to illustrate the relation of global laminate coordinate system (x,y,z) and local ply coordinate system (1,2,3) in terms of the fibre orientation angle ψ, picture taken from [Fla13]

1 Introduction

The usage of fibre reinforced polymers (FRPs) has been increasing in the last decades. Originally the usage of FRP's was restricted to specialised applications in aeronautics and astronautics. Nowadays, the usage of FRP's is more wide spread wherever their weight saving potential can be of advantage, due to their high specific stiffness and strength. Its applications have reached every day live, for example in automotive and sports industries and in conspicuous applications like wind turbine blades.

In applications were the load carrying capacity is critical and a failure of structural parts can have precarious outcome, reliable predictions of the onset of failure are crucial. But not only the onset of damage, plasticity and/or delamination has to be predicted, also its propagation is of interest. In typical applications of FRP, the layup consists of several unidirectional layers stacked in different orientations. Here, the maximum load carrying capacity of the structure might not be reached if a failure in one of the layers or between the layers occurs. In some cases the load can be increased significantly above the point of first ply failure (FPF) or the first occurrence of de-lamination. To predict the behaviour of structures beyond FPF and/or de-lamination, and therefore to exploit the full potential of FRPs, reliable simulation methods are needed. In most cases this simulation methods incorporate the use of the Finite Element Method (FEM), a numerical procedure to approximate solutions of differential equations. Two major approaches are in use, the implicit and the explicit method. The implicit method is mostly used for static applications, whereas the explicit FEM is advantageous for highly dynamic problems.
A constitutive law for the implicit finite element method (FEM) was developed by Flatscher [Fla10] at the ILSB. This material model for small strain, plane stress applications incorporates

- stiffness degradation, attributed to microscopic brittle matrix cracking, fibre/-matrix debonding, as well as progressive fibre failure, modelled via continuum damage mechanics, and

- unrecoverable strain accumulation, associated with the formation of microscopic areas with inelastically deformed matrix material, represented as a multi-surface plasticity law.

To account for the possibility of onset and propagation of delamination, the above material modell can, for example, be combined with cohesive elements, able to degrade and fail. In this combination every ply can be modelled separately with a layer of cohesive elements in between, joined together with a contact formulation. This means the non-linear material definition is combined with a contact definition, affecting big portions of the model. This combination can lead to severe convergence issues, when simulated with the implicit FEM. Another issue known from the work of Flatscher can be a long calculation time under certain circumstances, due to convergence issues within the material model itself. On the other hand the explicit FEM is known to have advantages when severe non-linearities in combination with contact definitions occur. Harewood and McHugh [Har06] have compared the implicit and explicit FEM using crystal plasticity. Their findings confirm that for certain loading conditions the explicit scheme may encounter less problems with convergence, and in conjunction with the high parallelization efficiency, can lead to a reduced calculation time compared to the implicit method. Another benefit can be a saving in required memory.

To exploit these possible benefits, the constitutive law from Flatscher is adapted to be used in conjunction with the explicit FEM. The existing implementation is an user subroutine for Abaqus/Standard (Dasault Systemes Simulia Corp., Providence, RI, USA). This subroutine called Umat was adapted into a Vumat, a subroutine for Abaqus Explicit. To investigate the advantages of the explicit method, some distinctive problems were simulated. These include a three point bending tests as well as open hole tension tests, a common structure for example investigated by Hallett et al. [Hal09]. Another example to investigate the potential concerning numerical stability is an unit cell from Jakob Gager [Gag13].

2 Explicit FEM

The Finite element method (FEM) is nowadays in widespread use to simulate the mechanical behaviour of structures. It's main advantage is the possibility to simulate structures for which the analytical methods are not suitable due to the geometry of these structures. The FEM can be described as a numerical method to solve differential equations. In its most common form an implicit discretization is used, where the solution for the later time $(i+1)$ in figure 2 of the underlying equation is calculated from state of the system at the later time $(i+1)$. This approach enforces the inversion of the stiffness matrix and an incremental approach for solving non-linear problems.

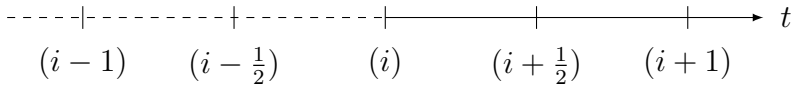

Figure 2: Sketch of a time-line, (i) refers to the current time, $(i-1)$ and $(i-\frac{1}{2})$ refer to earlier times and $(i+1)$ and $(i+\frac{1}{2})$ refer to later times.

The explicit FEM on the other hand calculates the solution for the later time $(i+\frac{1}{2})$ and $(i+1)$ of the underlying equation from the state of the system at current time (i) and at earlier times $(i-\frac{1}{2})$ and $(i-1)$. This leads to an entirely different solution method compared to the implicit scheme, as well as a different underlying equation. The explicit FEM is usually used to simulate highly dynamic problems like impact and wave propagation problems. It can also be applied to highly non-linear problems, were for example material non-linearities and contact occur simultaneously, due to its robust formulation. The underlying equation of the explicit FEM is given in [Bat02] in a well known form as

$$\mathbf{M}\ddot{\mathbf{u}} + \mathbf{D}\dot{\mathbf{u}} + \mathbf{K}\mathbf{u} = \hat{\mathbf{F}} \quad , \tag{2.1}$$

where $\mathbf{M}$ is the mass matrix, $\mathbf{D}$ is the damping matrix, $\mathbf{K}$ is the stiffness matrix and $\hat{\mathbf{F}}$ is the force vector. $\mathbf{u}$ is the nodal displacement vector with its derivatives with respect to time, $\dot{\mathbf{u}}$ and $\ddot{\mathbf{u}}$.

In the further considerations the damping matrix is assumed to be zero.

2.1 Algorithm

To describe equation (2.1) in form of a numerical code it is necessary to choose a discretization method which should enable a stable and computational efficient way of simulation. In the program Abaqus, which is used in this thesis, the time derivatives of $\mathbf{u}$ are discretized with a central difference scheme. This scheme uses two states from previous increments to explicitly predict the state of the current increment. The time at witch the expressions are evaluated is expressed with the superscripts corresponding to the current time (i), the last timestep $(i-1)$ the next timestep $(i+1)$ and two intermediate times $(i \pm \frac{1}{2})$. The time increment Δt is given by $\Delta t = t^{(i)} - t^{(i-1)}$. With the assumption of constant time increments this scheme can be written (after [Aba10])

$$\ddot{\mathbf{u}}^{(i)} = \frac{1}{\Delta t}[\dot{\mathbf{u}}^{(i+\frac{1}{2})} - \dot{\mathbf{u}}^{(i-\frac{1}{2})}] \quad . \tag{2.2}$$

The second derivative at time (i) is expressed in terms of the first derivatives at time $(i-\frac{1}{2})$ and $(i+\frac{1}{2})$, which can be expressed as:

$$\dot{\mathbf{u}}^{(i+\frac{1}{2})} = \frac{1}{\Delta t}[\mathbf{u}^{(i+1)} - \mathbf{u}^{(i)}] \tag{2.3}$$

$$\dot{\mathbf{u}}^{(i-\frac{1}{2})} = \frac{1}{\Delta t}[\mathbf{u}^{(i)} - \mathbf{u}^{(i-1)}] \quad . \tag{2.4}$$

This leads to the complete discretization scheme, where the second derivative of $\mathbf{u}$ is described by $\mathbf{u}$ itself. This scheme is also known for example in fluid mechanics, where explicit formulations are in wide spread use.

$$\ddot{\mathbf{u}}^{(i)} = \frac{1}{\Delta t^2}[\mathbf{u}^{(i+1)} - 2\mathbf{u}^{(i)} + \mathbf{u}^{(i-1)}] \tag{2.5}$$

If this discretization scheme is inserted in equation (2.1) and some of the terms are rearranged to express the unknown state $\mathbf{u}^{(i+1)}$ on the left hand side, it leads to:

$$(\frac{1}{\Delta t^2}\mathbf{M})\mathbf{u}^{(i+1)} = \hat{\mathbf{F}} + (\frac{2}{\Delta t^2}\mathbf{M} - \mathbf{K})\mathbf{u}^{(i)} - (\frac{1}{\Delta t^2}\mathbf{M})\mathbf{u}^{(i-1)} \quad . \tag{2.6}$$

The right hand side can be written in a shorter form expressed as $\hat{\mathbf{F}}$, the applied load vector and $\hat{\mathbf{I}}$, the internal force vector, giving rise to

$$(\frac{1}{\Delta t^2}\mathbf{M})\mathbf{u}^{(i+1)} = (\hat{\mathbf{F}} + \hat{\mathbf{I}}) \quad . \tag{2.7}$$

The algorithm can now be written in the form as being executed in Abaqus/Explicit. The terms are computed in sequence of the numbers over the equality sign in the equations (2.8 to 2.10) as stated in [Aba10]. The force vectors $\mathbf{F}$ and $\mathbf{I}$ are also known.

$$\mathbf{u}^{(i+1)} \overset{(3)}{=} \mathbf{u}^{(i)} + \Delta t \dot{\mathbf{u}}^{(i+\frac{1}{2})} \tag{2.8}$$

$$\dot{\mathbf{u}}^{(i+\frac{1}{2})} \overset{(2)}{=} \dot{\mathbf{u}}^{(i-\frac{1}{2})} + \Delta t \ddot{\mathbf{u}}^{(i)} \tag{2.9}$$

$$\ddot{\mathbf{u}}^{(i)} \overset{(1)}{=} \mathbf{M}^{-1} \cdot (\mathbf{F} - \mathbf{I})^{(i)} \tag{2.10}$$

Equation (2.10) originates from equation (2.1), with $\mathbf{D} = \mathbf{0}$ and $\mathbf{I} = \mathbf{Ku}$ and equations (2.9) and (2.8) are rearrangements of equations (2.3) and (2.2) respectively. From this set of equations it can be seen, that only the mass matrix has to be inverted. Other than that, only simple operations have to be done. The main advantage of the explicit scheme is that the consistent mass matrix can be approximated by a tridiagonal or lumped mass matrix. This approximation is the reason that linear elements are commonly used. This matrix can now be inverted very effectively using a TDMA (TriDiagonal Matrix Algorithm) algorithm.

Because of the use of the previous state ($\dot{\mathbf{u}}^{(i-\frac{1}{2})}$) in calculating the next state a special starting procedure is required. In Abaqus this is done by setting the velocity at the beginning to zero, unless otherwise specified by the user.

The central difference algorithm is consistent with a truncation error of $\mathcal{O}(\Delta t^2)$ as stated in [Bat02] .

2.2 Stability

The numerical stability of an algorithm is mostly defined by its behaviour to round off errors and other inaccuracies, occurring during calculation. These round off errors limit the accuracy of the solution. If the error in the solution accumulates significantly the algorithm is normally called numerical unstable. If the error in the solution is neglectable the numerical method is called stable. A detailed discussion of the derivation of the stability criterion can be found in [Bat02].

The commonly used implicit FEM is usually unconditionally stable, the 'time' increment is only limited by the accuracy needed. For explicit algorithms one strong limitation of the time increment Δt comes from the CFL (Courant Friedrich Lewy) criterion that has to be satisfied for every element at all times. This criterion can be approximated by

$$\Delta t < \Delta t_c \approx \frac{L_{min}}{c_d} \quad , \tag{2.11}$$

where Δt_c is the critical time increment, L_{min} is the smallest element dimension in the mesh and c_d is the dilatational wave speed, see [Aba10]: section 6.3. c_d can be defined for isotropic materials as

$$c_d = \sqrt{\frac{E}{\rho}} \quad . \tag{2.12}$$

For anisotropic materials the dilatational wave speed is not straightforward to calculate, also the smallest element dimension L_{min} is of interest. In most implementations, the stable time increment is approximated, and a safety factor is introduced. The stability limit, although it has to be evaluated locally, applies globally. It is depended on the element dimensions and the material characteristics stiffness and density, as obvious from equation (2.11) and (2.12).

2.2.1 Mass scaling

The stability limit of the algorithm acts as a global limit, meaning the biggest time increment to choose for all elements is determined by the one element with the smallest stable time increment. This means a few very small and stiff elements with low density can increase the calculation time significantly. To reduce the calculation time it is possible to raise the density of these few small elements in order to raise the stable time increment. It can be seen in equation 2.12 that in order to raise the stable time increment by a factor of f the density is raised by a factor of f^2.
This option should be applied with care, because it alters the solution by adding artificial mass to the model. Nevertheless, if the added mass is small the dynamic response is not altered too much and the calculation time can be lowered significantly.

2.3 Accuracy

In the explicit integration scheme used, one suitable way for the user to monitor the accuracy of the solution, is to monitor the energy balance, meaning the conservation of energy. If the time increment is sufficiently small, the energy balance is off by a very small fraction (normally lower $\mathcal{O}(-3)$) compared to other energies, like the strain energy, due to numerical round off errors. With the time increment getting bigger the error in the energy balance is getting bigger, suggesting the chosen time increment is too big. The clue is to find a time increment satisfying the accuracy requirements and also allowing a decent calculation time.

This condition may vary over the time simulated, so it can be of advantage to set the time increment dependent on the error in the energy balance. It is possible to use the built in capability of most FEM programs to automatically adjust the time increment, if applicable. Otherwise an iterative approach by the user is required, first calculating a solution with an estimated time increment and then restarting or repeating the analysis with an adapted time increment, possibly varying over time.

2.4 Quasi-static problems

The explicit FEM is most often used to simulate transient problems on very small time scales, for example ballistic impact and crash analyses. Another advantage is the possibility to handle severely non-linear behaviour, like non-linear material behaviour in combination with interface and contact definitions, as carried out in this thesis. The explicit scheme can be used to simulate quasi static problems by choosing the simulation time (the loading rate) in a way that the dynamic influences don't disturb the solution (mostly named load rate scaling). The choice of this simulation time is tricky, because a decent calculation time depends strongly on the time simulated. One statement is available in nearly every literature. It reads, 'the value of the kinetic energy should not exceed a small fraction of the value of the strain energy', stated in [Aba10] or [Nas10]. However, its meaning has to be evaluated by performing simulations with different loading rates. An initial guess can be obtained via the eigen-frequencies of the model see for example [Par66].

Particular attention needs to be turned to changes in loading speed, for example at the start of an analysis. To avoid dynamic influences, like vibrations, the load should be applied as smooth as possible, meaning the time derivatives of $\mathbf{u}$ should be kept as small as possible. The time increment chosen for such analysis is most likely close to the stability limit, because the high simulation time enforces a high number of time increments.

3 Elasto-Plasto-Damage-Constitutive Law from Flatscher [Fla10]

The present work is based on the work of Flatscher [Fla10], and Schuecker [Sch05]. A short survey of the constitutive model is given below, for more information the reader is refereed to the original thesis. Some additional information can be obtained from [Fla13] and [Fla12].

In the following chapter the constitutive law from Flatscher [Fla10] is reviewed. The smeared out material model applies to plies that are embedded in a laminate only. As it applies to thin walled, laminated components, the plane stress assumption is justified. The material properties as well as the damage and plasticity mechanism are modelled in an average sense, the implementation is done traversal isotropic.

Distributed brittle damage accounts for the stiffness degradation due to microscopic brittle matrix cracking and fibre matrix de-bonding. The strains accompanied by this phenomena are taken to be recoverable after unloading, therefore refereed to as elastic strains. In this approach no localization is expected, so strain hardening is modelled. Localized brittle damage, leading to damage and strain localization in structural analyses. Multi-surface plasticity accounts for the accumulation of unrecoverable strains and is associated with inelastic microscopic matrix deformation. The strains accompanied are termed plastic strains.

To combine the outlined approaches in one single constitutive law, the elasto-damage model is enriched by the plasticity model. So for an integrated loading history the strain decomposition reads

$$\boldsymbol{\varepsilon} = \boldsymbol{\varepsilon}^{\mathrm{el}} + \boldsymbol{\varepsilon}^{\mathrm{pl}} = \mathbf{C}\boldsymbol{\sigma} + \boldsymbol{\varepsilon}^{\mathrm{pl}}. \tag{3.1}$$

The term $\boldsymbol{\varepsilon}$ is the vector of mechanical strain components, $\boldsymbol{\varepsilon}^{\mathrm{el}}$ is the vector of the elastic strain components and $\boldsymbol{\varepsilon}^{\mathrm{pl}}$ is the vector of the accumulated plastic strain components. $\mathbf{C}$ is the current compliance matrix, possibly altered by damage and $\boldsymbol{\sigma}$ is the vector of stress components. The compliance matrix $\mathbf{C}$ and the vector of plastic strain components $\boldsymbol{\varepsilon}^{\mathrm{pl}}$ determine the non-linear behaviour, their evolution is given by incremental formulations. Some crucial assumptions are based on work of Puck [Puc96] on FPF. These findings are not reviewed in detail.

3.1 Distributed brittle damage

This section follows [Fla10], were detailed considerations can be found. This part of the material model is formulated by embedding fictitious inhomogeneities into the undamaged but smeared out ply material. In this way it is possible to describe the anisotropic characteristics of matrix related damage by using only scalar variables. The initiation of damage is directly related to Pucks failure surface for plane stress [Puc96]. A factor of matrix exertion $f_E^{(m)}$ is introduced which depends on the current stress state only. It reaches the value of one when Puck predicts FPF, and is used to govern the evolution of damage. The evolution of the damage state is, of course, a function of the ply loading history, meaning an large number of possibilities exist. Due to the approach of using fictitious inhomogeneities, a method borrowed from micro-mechanics, the fourth order elasticity tensor of the damaged ply can be predicted by using only scalar variables. To account for the different loading cases three populations of inhomogeneities are introduced.

The three fictitious inhomogeneities can each be described via their shape (i), volume fraction (ii), orientation (iii), and assigned material properties (iv), although these inhomogeneities are not intended to represent actual cracks.

(i) The shape of the inhomogeneities are oblate spheroids, their axis of rotations is aligned with the fracture plane normal predicted by Puck [Puc96]. With the choice of this shape the anisotropic characteristic of the modelled damage is defined. Known

from experimental results, penny-shaped voids are suitable, the shape remains constant throughout the analysis

(ii) The volume fraction $\xi^{(m)}$ of the fictitious inhomogeneities is directly related to the amount of damage. An evolution equation is postulated which assumes that the amount of damage is related to the factor matrix exertion.

(iii) The orientation of the penny-shaped inhomogeneities is assumed to be directly related to the fracture angle predicted by Puck. For loading conditions resulting in a fracture plane angle of $\varphi = 0$ (see figure 3), the axis of rotation of the inhomogeneities is defined parallel to the in plane transverse direction of the ply. If a fracture plane angle of $\varphi \neq 0$ is predicted, the orientation is tilted by the same angle. In general, non-radial loading conditions are also considered, as well as unloading conditions, but are not recapitulated here.

(iv) The voids are modelled with material properties dependent on their current stress state. This way it is possible to account for differences in tension and compression as well as frictional effects.

Three populations of inhomogeneities are introduced, their superposition accounts for general stress states and loading histories. The above mentioned variables are used to determine the full tri-axial compliance tensor for the damaged ply material, using a Mori-Tanaka-like method.

3.2 Multi-surface plasticity

This section follows [Fla10], were detailed considerations can be found. For a more detailed introduction to plasticity mechanisms the reader is refereed to [Dun05].

Laminates exposed to in-plane shear or transverse compression are known to accumulate unrecoverable strains. This behaviour is captured by a phenomenological model assuming that plastic shear strains are driven by tractions acting on planes, called 'shear planes' in the following, which are similarly oriented as Puck's fracture planes. To circumvent some difficulties with the unknown and changing orientation of Puck's fracture planes two plasticity mechanisms are incorporated, each of which is driven by

a characteristic shear component assigned to a shear plane. Both of these mechanisms can be active at the same time, allowing for a general behaviour.

In-plane shear Under dominant ply shear loads the Puck criterion predicts a fracture plane angle of $\varphi = 0$ (see figure 3), therefore it is assumed, that plastic shear strains $\gamma_{12}^{(\mathrm{pl})}$ accumulate. The main driving force is the shear stress component σ_{12}, but σ_{22} also influences the evolution of plastic strain via three interaction parameters.

Transverse compression For load states leading to inclined fracture plane angles according to Puck, it is assumed that plastic shear strains $\gamma_{nt}^{(\mathrm{pl})}$ are accumulating on inclined shear planes. These are primarily driven by the stress component σ_{nt}, with influences of σ_{nn} and σ_{ln}. This mechanism is formulated in the ply coordinate system where the plastic strains $\varepsilon_{22}^{(\mathrm{pl})}$ and $\varepsilon_{33}^{(\mathrm{pl})}$ accumulate under dominate influence of σ_{22} also affected by σ_{12}

Both of the above mechanisms are described by a yield condition, a flow rule and a hardening law. The needed consistency conditions as well as the loading-unloading conditions are left out for the sake of brevity. The interaction of the two plasticity mechanisms is addressed in section 3.4.

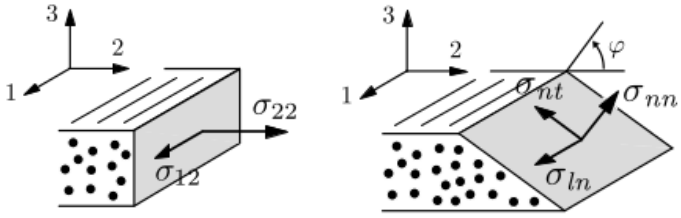

Figure 3: Sketch of the 'shear plane' of the two plasticity mechanisms, 'in-plane shear' with an angle of $\varphi = 0$ (left) and 'transverse compression' with an angle of $\varphi \neq 0$ (right), taken from Flatscher [Fla10].

3.3 Localized brittle damage

To complete the formulation of the material law, the possibility of softening and localized failure, the formation of locally disintegrated areas or even discrete cracks in structures is addressed. To this goal it is not sufficient to focus on matrix dominated issues, as done in the above sections, but also fibre dominated phenomena are to be addressed. Localized failure is modelled as local stiffness degradation accompanied by strain softening behaviour in the sense of brittle continuum damage mechanics. The outlined model from section 3.1 is picked up and a fourth population of fictitious inhomogeneities is introduced to capture the progressive fibre failure. These fictitious inhomogeneities have a constant spheroidal shape, with the axis of rotation aligned with the fibre direction. The relation of damage and effective stiffness is the same as in section 3.1, the onset of softening is assumed when the factor of fibre extension $f_E^{(f)}$, again related to Pucks findings on FPF, reaches a value of one. For matrix dominated phenomena it is assumed that softening behaviour initiates only after a certain, material dependent, amount of matrix damage has accumulated, resulting in $f_E^{(m)} > 1$ at onset of softening.

For the definition of the damage evolution, the multi-axial stress and strain states are reduced to scalar ones by introducing equivalent stresses and strains. Four different modes, fibre tension, fibre compression, matrix tension, and matrix compression are distinguished, where the in plane shear behaviour is captured in the latter two. For the softening regime, exponential softening is assumed. Localized failure is modelled in the form of an equivalent stress equivalent strain relation. In this context the use of the energy dissipated per unit sectional area failing is needed. Its disadvantageous influences are reduced by the use of a characteristic length, dependent on the local element size. The amount of damage is linked to the equivalent strain, and the stiffness matrices are calculated similar as in section 3.1.

For the use in conjunction with an implicit FEM program such as Abaqus/Standard the use of viscous regularisation can improve convergence significantly. Viscous regularization is defined as a rate equation for the damage variables. This approach does

not influence the results significantly as long as the viscous parameters are chosen sufficiently small. This can be checked with the energy dissipated due to viscous effects. If they are small enough, their influences, in particular the slowing down of the rate of damage and the retardation of localization, are kept to a minimum.

3.4 Implementation

The constitutive law described above has been implemented by Flatscher [Fla10] in an user subroutine for the FEM package Abaqus/Standard, called Umat, written in Fortran. Given below is a general outline of the iterative procedure, executed in every call of the Umat. It is structured in three levels, starting with level zero.

- Level 0: The state of the needed variables are read from the last Call of the Umat, switches and parameters are set. If necessary, the strain increment is divided into equal sub-increments: $\Delta\varepsilon = \sum \Delta\Delta\varepsilon$. For every strain sub-increment $\Delta\Delta\varepsilon$ Level 1 is called.
  - Level 1: Based on the given strain sub-increment (or the solution from the last call of level 2), a pre-estimate of the damage state is calculated. With this damage state Level 2 is called.
    - Level 2: A Predictor-Corrector algorithm is used in the following way: First an elastic trail stress is used to pre-estimate the active plasticity mechanism. Based on this assumption, the stress state of the set of active plasticity mechanism(s) (one (or two) yield condition(s) and flow rule(s)) is solved iteratively. The found state is checked whether the assumption on the active mechanism was correct, and if the internal hardening variable(s) is (are) non negative. If the above assumption was not correct, a different set of active mechanisms is assumed and Level 2 is repeated.
  - Level 1: The solution from Level 2, which is converged for the plasticity model, is checked whether the damage state is expected to change. If so,

the iteration scheme can be outlined as:

$$F[\,{}^{n-1}\xi^{(m)}] - {}^{n}\xi^{(m)} = 0, \tag{3.2}$$

where n denotes the number of iterations and $\xi^{(m)}$ is the damage variable. With the new damage state Level 2 is called again, until a truncation condition is met.

- Level 0: At the end of the main iteration the state of the non-viscous system is known. The state of the viscous system is calculated next, if required. Then the material Jacobian matrix along with other useful quantities, like engineering elastic constants, factors of exertion, energy densities,etc. , are computed. If errors occurred, the error massages are written to the *.msg file. The Variables are updated and a single call of the Umat is closed.

Limitations

A few limitations arise from the implementation, being the restriction to small strains and the plane stress assumption.

4 Implementation of the EPD model in Abaqus/-Explicit

The constitutive law from Flatscher [Fla10] was implemented as an user subroutine for Abaqus/Standard, called Umat. The goal of the written Vumat, a subroutine for Abaqus/Explicit, is to include the Umat itself as a subroutine. This makes the EDP model applicable to explicit simulations. Furthermore the input and output of an Umat and a Vumat differ, thus some variables have to be adapted. Also in the beginning of an analysis, some modifications have to be made, to account for initial calculations made by Abaqus/Explicit. In detail the Vumat is called first in single precision (meaning the subroutine is compiled twice) for the calculation of the initial stable time increment. Here a set of fictitious strains are given and the corresponding stresses have to be cal-

culated purely elastic.

There are some differences in the sense of how often the subroutine is called. In Abaqus/Standard the subroutine is called a couple of times for every material point and time increment. The Vumat is called just once for every increment, but the number of increments is by far higher compared to the implicit scheme. Therefore some modifications concerning the output written to file were made.

4.1 Implementation

The user subroutine Vumat is written in Fortran (see for example [Bau03]), according to the Abaqus manuals (see [Aba10] and [Aba11]). The main difference is that an Umat is often called more than once for each material point, whereas a Vumat is called for several material points at the same time, allowing for a better performance in parallel computing. Another difference between Umat and Vumat, is from a programming point of view, the ordering of the tensor components and the procedure at the beginning of the analysis.

The tensors are stored in mathematical vectors containing the tensorial components in different order. In an Umat the order is [11 22 12], in a Vumat the same tensors are given as [11 22 33 12], for plane stress applications. Also the strains and strain increments are given in tensor components in a Vumat and in engineering components in an Umat. Due to the small strain assumption of the Umat the components just have to be rearranged and the shear strain component(s) multiplied/divided by 2. Particular attention should be paid whether the quantities are given at the end or the beginning of the increment. In an Umat the vector of stress components for example is given as input at the beginning of the increment and has to be updated to be the vector of stress components at the end of the increment. In a Vumat two vectors of stress components are given, one as an 'old' vector of stress components at the beginning of the current increment and one as a 'new' vector of stress components, which has to be written, containing the values at the end of the increment. Also the time is given to the subroutines at the beginning or end of the increment for an Umat or a Vumat, respectively.

A Vumat should normally be compilable in single and double precision, allowing for single or double precision analyses. Because the given Umat is hard coded in double precision, it was decided to allow only double precision analyses. As the calculations carried out in the Vumat, account for the bulk of the computational time, this has just minor effects on the computational performance. In an Abaqus user subroutine the storage of variables is done via solution dependent variables. Since there is no space accommodated to store the strain components in a Vumat, the number of solution dependent variables (SDV's) is increased. Finally the internal energy and the dissipated energy per unit mass at each material point at the end of the increment has to be calculated from the energies calculated in the Umat and the material density.

So basically, the Vumat acts as directory, rearranging the Input and Output of the UMAT to fit the expectations. It can be outlined like in section 3.4, with the VUMAT as level -1:

- Level -1: (Vumat): The input variables of the Vumat are rearranged as described above and the Umat is called
  - Level 0: (Umat): See section 3.4; Some alterations had to be made concerning the error output to the .msg file, much of it is suppressed, and the calculation of the Jacobian is suppressed, as it is not needed in Abaqus/Explicit.
- Level -1: (Vumat): The Output of the Umat is again rearranged.

The viscous parameters, introduced in Flatschers material law, have to be adapted to the changed time scale in explicit simulation. These parameters can be approximated in terms of loading rate, by scaling them linearly. In implicit simulations the time is normally set to one and the load is raised linear to the maximal bearable load. In explicit simulations the load is applied at a much smaller time scale and does not vary linear with time. Therefore it is advised to take the load rate at the first appearance of softening for the scaling of the viscous parameters.

Due to the fact, that not all the input quantities given to the Umat are available in a Vumat, some error messages and variables are of no meaning in Abaqus/Explicit. This concerns the numbers of elements, integration points and section points as well as the number of increments and the number of the current step.

4.2 Verification, single element tests

The solutions are first verified with tests on single linear reduced integrated conventional shell elements, namely S4R elements, with displacement controlled loading in all three directions (two principal components and one shear components, 11 22 12 in Abaqus notation), and periodic boundary conditions. A lot of different simulations with similar input parameters for implicit and explicit FEM are carried out, using the original Umat and the Vumat containing the Umat. The results in terms of stresses agree within one percent accuracy. Other variables were monitored too, they match within the given tolerance but are not described in detail. Other loading scenarios were also captured in this verification scheme with satisfactory agreement, but are left out for the sake of brevity.

For this verification scheme, the time increment is chosen in a way that the energy balance is nicely fulfilled, meaning the deviation in the energy balance is lower than 1.0 e-5. The load is applied in increasing smooth steps (pulsating load). Alternating loads can only be applied if softening is not active, because in this regime the algorithm of the Umat is strain based and does not account for alternating loading paths.

An example of a loading path is shown in figure 4, the strains are given and the resulting stress-components from Abaqus/Standard and -/Explicit are shown in figure 5. It can be seen that the results in terms of stresses are nearly coincident.

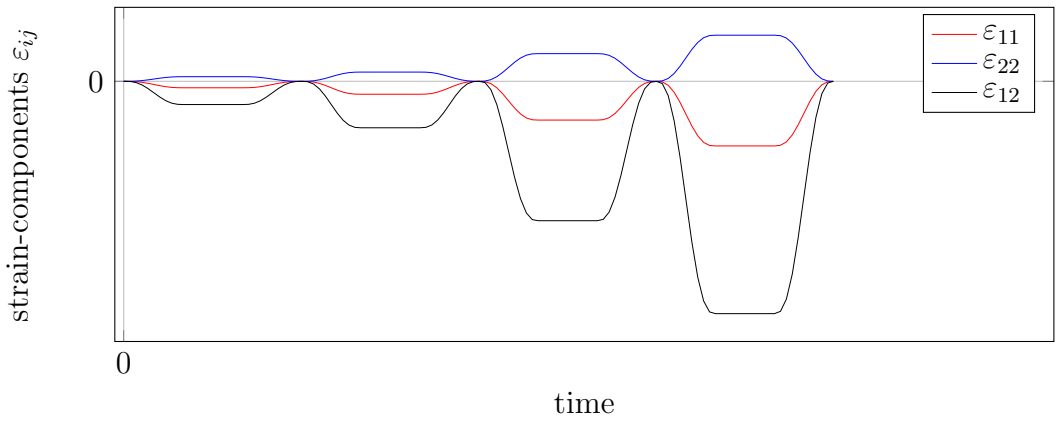

Figure 4: Exemplary strain components used as load for the verification of the user subroutine.

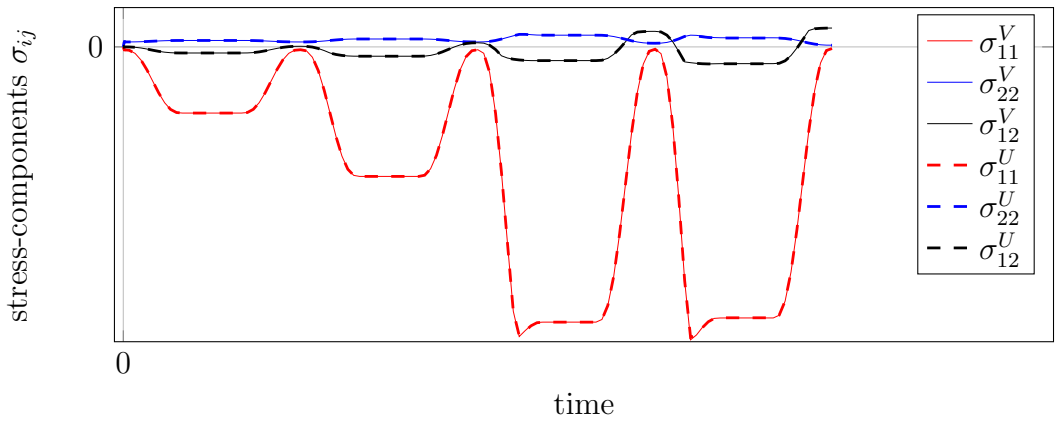

Figure 5: Stress components as response to the strain components in figure 4 obtaind from Flatschers Umat (σ^U_{ij}) as well as from the current Vumat (σ^V_{ij}).

4.3 Limitations

The limitations of Flatscher's material model and its implementation (see section 3.4) are still valid, some known problem of the Vumat are discussed next.

The estimation of the stable time increment in conjunction with the Vumat is not as accurate as expected. It turns out that the stable time increment is overestimated, depending on the orientation of the fibres in the ply. This behaviour is especially unsuited in conjunction with the option mass scaling for quasi-static simulations. A simple workaround is provided in Appendix A to circumvent problems associated with this behaviour.

Sometimes a not assignable error ('signal 11') occurs if jobs are run in parallel. No workaround has been found, in most cases this error still occurs even if the Vumat is not used. It is assumed that it is a problem of Abaqus and not of the Vumat in particular.

The viscous regularisation is not necessary to ensure convergence of the algorithm in explicit FEM. If simulations are to be compared to the implicit FEM the viscous parameters are best linearly scaled by the loading rate. The influence of the viscous regularisation should be examined thoroughly, as it is was introduced in the original implementation for numerical issues only. The known influences are increases in peak stresses, the slowing down of the rate of damage accumulation and the retardation of localisation. This influences can compromise the solution in an explicit FEM program as dynamic influences can occur. In such an event one has to carefully investigate the influence of the viscous regularisation, because the propagation of a localization zone may be influenced.

5 Applications

After the development and implementation of a constitutive law, one is eager to apply it to a real structure. To this end three Applications are chosen. The first one is a simple three point bending specimen. Here some characteristics of Flatscher's EDP-model can be shown. The main part of this section is devoted to open hole tension tests. This application is used to show the capabilities of the current material model in conjunction with the explicit integration scheme. In the last part of the section a model of the Ph.D.-thesis of Jakob Gager [Gag13] is used to show the capabilities of the current implementation.

5.1 General modelling

In this thesis one particular approach is chosen to simulate laminated fibre reinforced composites. This approach consists of the usage of shell elements to model the individual plies and cohesive elements to model the interfaces in between. Four-noded shell elements are used, they are reduced integrated with five section points in the thickness direction applying the simpson rule integration. The constitutive model used with these shell elements is, of course, the current EPD-model. The two material system under consideration are carbon/epoxy systems called Cycom977 and RTM6/HTS40, the material parameters can be found in [Fla10], see Appendix C, table C.1 to C.7, page 121 to 124 and [Gag13]. The reduced integration requires hourglass control, which is chosen as the standard option, known to Abaqus users as 'enhanced hourglass control'. The shell elements in use require the manual definition of the transverse shear stiffness, which is calculated according to the Abaqus Manual [Aba10] section 29.6.4. The transverse shear components have approximate character and are only evaluated at the beginning of the analysis. This means for applications where the transverse shear stiffness is of big influence the usage of the current approach might be questionable, even though every ply layer is modelled individually.

The interfaces are modelled with cohesive elements, a special purpose element in the element library of Abaqus, coupled to the shell elements via a Tie constraint. They

exhibit a stiffness in thickness direction (z according to figure 1) as well as in two transverse shear directions (zx and yz according to figure 1). Their constitutive behaviour is described by a traction-separation response, the possibility to exhibit damage and failure. The initiation of damage is described by a quadratic stress criterion. Its evolution is described by the energy dissipated by the damage process, the mode mix is described by the Benzeggagh-Kenane fracture criterion with an exponent of 2. Damage stabilization is not required. The stable time increment is not affected by the geometrical thickness of the interfaces as a result of the traction separation response. Their geometrical thickness can be set very small values of 1/100 of the ply thickness, to model the zero thickness interface. The thickness direction has to be assigned manually to ensure a proper behaviour. Elements are removed once the maximum damage is reached. The properties of the cohesive elements are taken from [Gag13], see Apendix A, table A.3, page 112.

5.2 Three point bending test

In this section simulations of three point bending specimens are carried out. The set-up is shown in figure 6. It consists of two supports at a given distance, one punch in the middle of the specimen and a strip of [0/90] laminate in between. The center punch is lowered and the response of the specimen is investigated. The problem is modelled as follows: The supports and the punch is assumed to be rigid and therefore modelled as rigid surfaces. The contact is modelled with a friction coefficient of 0.3. The specimen, a laminate with two plies (t=0.75 mm) in orientations of zero and ninety degrees, is modelled with one shell element each in its width, meaning in z-direction an infinitely wide strip is modelled. The boundary conditions applied assure that no out of plane displacement and rotations occur. Although the single plies are too thick to be manufactured as one ply, the current model does not account for ply thickness effects, so the two (stacked) plies are modelled as one ply each. The material is Cycom977, the material parameters are given in [Fla10]. Two quasi-static explicit simulations are carried out, one with the EPD-model adapted for the explicit scheme (called 'Vumat')

and one with the built in material model from Abaqus. As the EPD-model is written in a small strain, plane stress formulation, it can give an idea of the applicability of the EPD-model when large rotations are evident. For the use of the Abaqus material *Elastic Type=Lamina (called 'Abaqus material'), the damage initiation law is based on Hashin's theory. The evolution of damage is defined in terms of the energy required for failure (fracture energy) specified as a function of the mode mix by means of the Benzeggagh-Kenane mixed mode fracture criterion. The same material parameters are used as in the EPD-model, but not all of them, arguably. The Interface is modelled with cohesive elements, as described in section 5.1.

Due to the nature of the problem load rate scaling is only applicable to a certain level. This results in a high number of increments and a high calculation time. The global behaviour in terms of reaction force acting on the punch versus displacement of the punch is shown in figure 7 for both models. They roughly coincide until the damage initiation criterion is met. The reasons for the differences occurring prior to damage

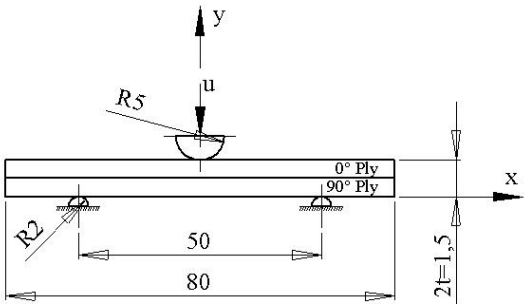

Figure 6: Sketch of the three point bending specimen and its dimensions in mm, the thickness of the plies is enlarged for better visibility

initiation is probably found in the fact that the EPD-model would only be applicable to small strain applications. But as large rotations of some elements are evident, the simulations are run in the non-linear geometry setting. In this setting a rotation of an element does not lead to strains and stresses in an element and also the rotation of the transversal isotropic material is accounted for. The strain increments in Abaqus are given into the EPD-model in a way that the only difference is the value of these increments due to the higher order terms in the calculation of the strain components.

But as the individual elements are only subjected to small strains, the error induced by this is only 0.5% in terms of strain value at damage initiation. The high frequent oscillations at the beginning are probably due to the contact definition, the manual refers to this behaviour as contact noise, see [Aba10]. The subsequent small oscillations are dynamic influences, although the kinetic energy is small compared to for example the strain energy. Some of the oscillations occur due to the initiation of damage at a displacement of $u \approx 1.7$ mm. In figure 8 the evolution of the damage initiation criterion for three locations in the 90 degree ply are shown in terms of a damage initiation factor.

The three locations are at x=0, the top of the ply at the interface (y=t), the middle of the ply (y=t/2) and the bottom of the ply (y=0). The distribution prior to damage onset is of no meaning, as the initiation factor are not defined the same way. The displacement as the initiation variables for the material point at y=0 reaches the value of one, associated with initiation of damage, is roughly the same for both material models, again due to the finite deformations setting. The evolution of damage differs for the material models as different evolution laws are used and due to the fact, that in Flatschers EDP model softening is delayed in matrix dominated damage phenomenon until the damage variable reaches the value of $\xi^{(m)} = 0.015$ for this material. Up to this point distributed brittle damage is assumed. Figure 9 shows the evolution of the damage variables, clear differences can be observed. This behaviour leads to the higher bearable load, when the Vumat is used. One can see when comparing figure 8 and 9, that the unstable damage growth, when the center element of the 90 degree ply gives way, is directly related to the point where the damage variable of the first material point, line a1) in figure 9, reaches the value of one. Once the first material point of the shell element gave way, the damage grows in an unstable manner. In figure 10 the specimen is shown shortly after the maximal load is reached. The center element of the 90 degree ply is damaged and some of the cohesive elements have failed, forming a de-lamination area. The response of the specimen after this breakage is highly dynamic and is not investigated further.

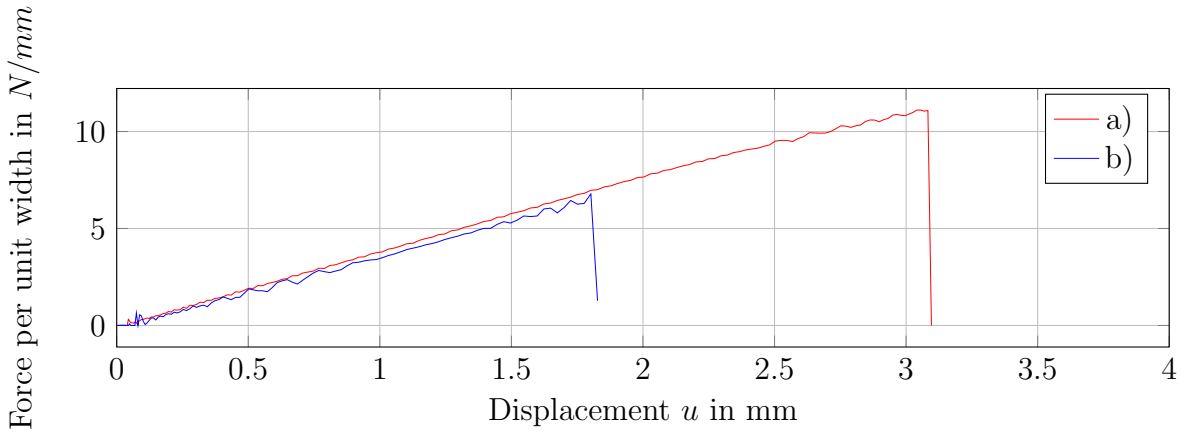

Figure 7: Global force per unit width versus global displacement u of the three point bending specimen, simulated with two material definitions a)the current Vumat and b) the Abaqus material.

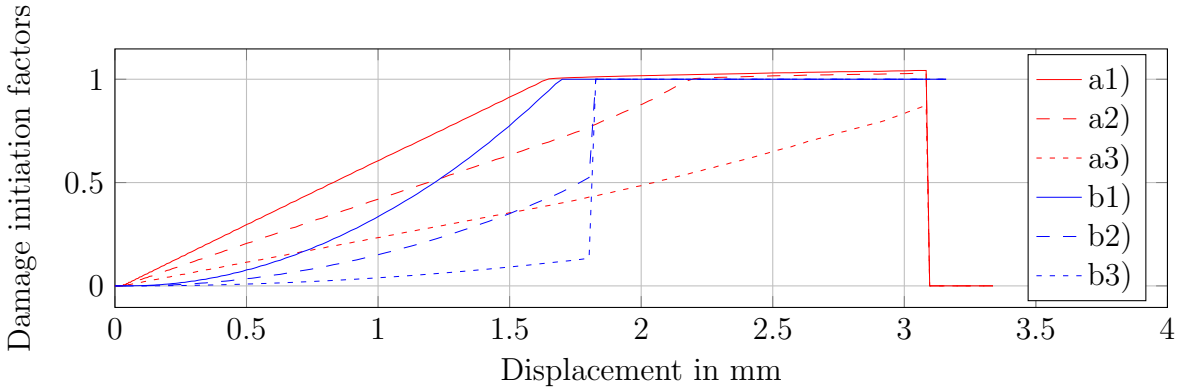

Figure 8: Damage initiation factors versus global displacement u of the three point bending specimen for the middle element at the bottom (1), middle (2) and top (3) of the 90 degree ply, simulated with two material definitions a)the current Vumat and b) the Abaqus material.

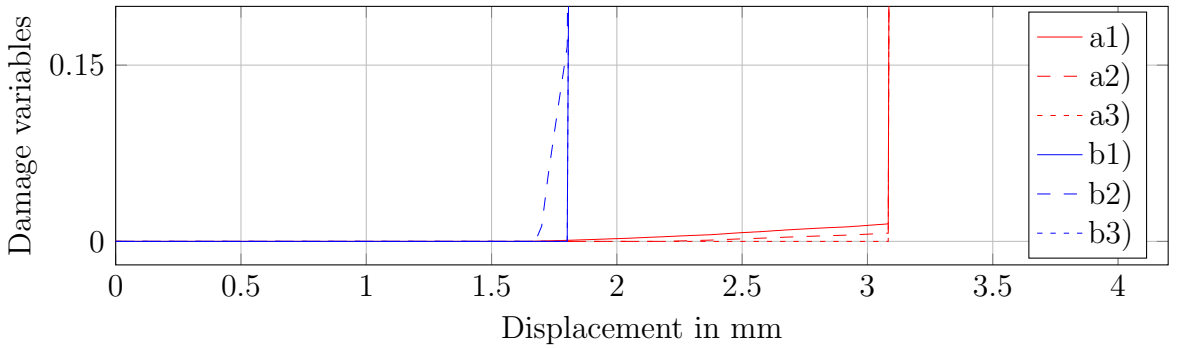

Figure 9: Damage variables versus global displacement u of the three point bending specimen for the middle element at the bottom (1), middle (2) and top (3) of the 90 degree ply, simulated with two material definitions a)the current Vumat and b) the Abaqus material.

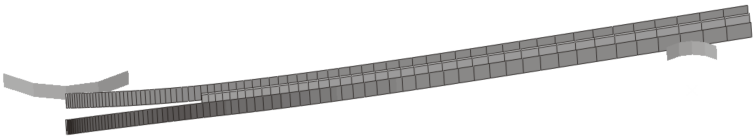

Figure 10: Three point bending specimen shortly after the maximal load, the center element of the lower ply has failed, as well as some of the cohesive elements, only one half of the model is shown.

5.3 Open hole tension tests

The following section addresses the application of the above described material model to open hole tension specimens under uni-axial tension in different layups. This specimens are chosen because they are investigated in various publications and experimental results are available for example from [Fla12]. Another reason to choose this particular specimen is the occurrence of the majority of the non linear effects captured in the current material model as well as the need for a robust solution method, in this case the explicit FEM scheme. In combination with the usage of cohesive elements delamination effects can be captured as well, giving rise to the interest of this particular specimen type.

In figure 11 the geometry is shown as well as the laminate and ply coordinate systems. The nominal dimensions are chosen as shown, resulting in ratios of $l_f/d \approx 20$ and $w/d \approx 5$, in accordance to the third World Wide Failure Exercise. With the usage of FEM models the need of discretization is immanent. In the explicit integration scheme only four-noded shell elements are available, due to the usage of the lumped mass matrix, see section 2.1. The integration method chosen is a reduced integration. As the majority of the calculation time is spent in the user subroutine (the material model) the loss in calculation speed is small when a higher number of reduced integrated elements is used compared to a lower number of fully integrated elements. Another advantage of the reduced integrated shell elements (S4R) lies in the post processing, because the color coding can be constant over the elements. The thickness of the elements is set to the thickness of the individual plies with five section points (integration points over

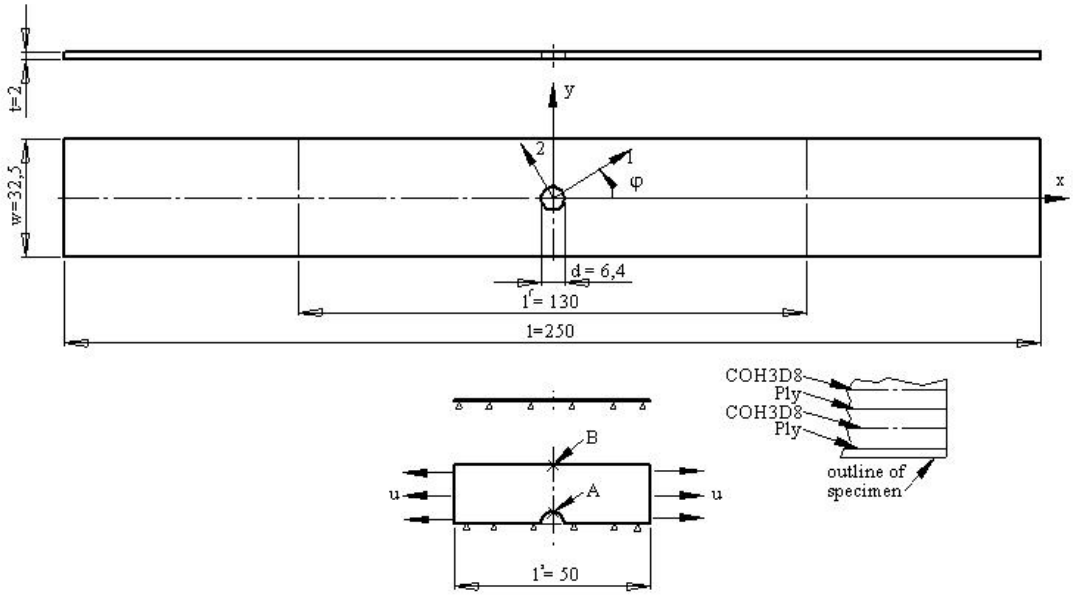

Figure 11: Sketch of the open hole tension test specimen with its dimensions in mm and the laminate coordinate system (top) and the shortened FEM model with indicated boundary conditions, layers of plies and interfaces (bottom)

the thickness of the shell element), with a simpson type integration method. The size of the elements varies over the area, with small elements (edge length about 0.03 mm) at the vicinity of the whole, because high stress gradients have to be resolved. Another reason for the size of the elements is the behaviour of the material model in the softening regime. Due to the small specific fracture energies for localized matrix failure, a fine FEM mesh is required at areas where softening takes place. If the mesh would be too coarse the stress strain curve would show a snap-back type shape. Due to the localized softening approach, and although a characteristic element length is used to reduce mesh size effects, it is good practice to choose the size of the elements affected by localization approximately equal. This requires an iterative user guided re-meshing approach to ensure equal mesh size in localization areas, as they are not known a priori. The individual plies are modelled as individual layers of shell elements with cohesive elements in between. The behaviour of these cohesive elements is the same as in section 5.2, again taken from [Gag13]. Residual stresses from the manufacturing process are simulated via a cool down from the approximated stress free temperature of 177 degrees Celsius to 20 degrees Celsius room temperature.

All the above mentioned lead to a very high number of elements, if the hole specimen with all its layers would be simulated. To reduce the computational time required in the FEM model symmetries are used, the model is shortened and only two layers are considered. As the geometry is symmetrical it might be possible to simulate only a part of the geometry. To do so it is necessary to ensure that the solution will also be symmetrically. The simulations showed, that this is only true for the symmetry about the x axis, about the y axis the solution is more or less symmetric, depending on the layup. One of the plies is constrained in its out of plane displacement, assuming it to be the ply next to the x-y symmetry plane. The load is applied in a displacement controlled manner, the left and right edge are displaced equally. As a explicit FEM is used to simulate quasi-static problems the calculation time is dependent on the load rate scaling, meaning the load has to be applied in a way that dynamic influences are kept to a minimum. To shorten the calculation time it is advantageous to shorten the length of the specimen, because the major dynamic influences result from longitudinal oscillations. This means that if the length is shortened by a factor of 2 the calculation time can be cut down by a factor of approximately 4. In all the simulations this approach was used, the specimen was shortened to a length of 50 mm. The results are not affected, as the major non-linear effects are restricted to the center of the specimen. This was verified by simulations without cohesive elements, with the use of shell elements with layered section definitions. The solutions published in [Fla12] could be reproduced. The third possibility to reduce calculation time is to simulate only some of the layers, assuming that the solution is the same for plies with the same orientation. This has to be postulated, and further investigations would be of great interest, because with the current approach it should be possible to capture some of the stacking influences.

For two of the layups under consideration experimental results are available, published by Flatscher et al, [Fla12]. Their experimental setup consisted of a computer-controlled servo hydraulic testing machine in laboratory environment and a 3D image correlation photogrammety system to obtain the strain fields. For further information on the setup and the used equipment the reader is refereed to [Fla12].

Results for layup $[0/90]_S$

The first layup under investigation is a $[0/90]_S$ laminate. As half of the fibres are oriented in loading direction, the specimen is very stiff. This enables the use of high load rate scaling, leading to relatively small computational time of 8.5 hours with a standard desktop Pc. In figure 12 a detail view of the mesh of the current specimen is shown. In the vicinity of the hole the mesh is very fine with a element length of approximately 0.03 mm. This areas extend in loading direction as previous simulations have shown that the localization zone extends in this direction.

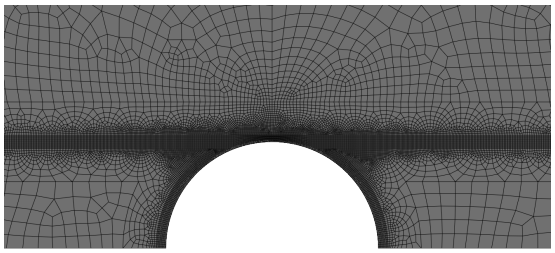

Figure 12: Detail view of the mesh of the $[0/90]_S$ *open hole tension test specimen*

The strain fields from the FEM simulation of the open hole tension test with a $[0/90]_S$ layup can be compared to experimentally determined strain fields due to the optical measurement published in [Fla12]. In this thesis the same material model (EPD from [Fla10]) was used in conjunction with the implicit FEM code Abaqus Standard, and shell elements with layered section definitions. The experimental results in terms of ply shear strain ε_{xy} are shown in figure 13 (top) and the results from the implicit simulations at a slightly different load level are in the same figure at the bottom. As already written in the original thesis [Fla12]: " ... the correspondence of the strain distributions is very good, a fact that suggests that important mechanisms are captured well by the present constitutive model.". In the current thesis the simulations are carried out with the explicit FEM code Abaqus/Explicit in conjunction with cohesive elements, representing the interface. The results in terms of ply shear strains are shown in figure 14, at the top for the 90 degree ply and on the bottom for the 0 degree ply. The strain distributions for the two separate plies are nearly equal, only near the top

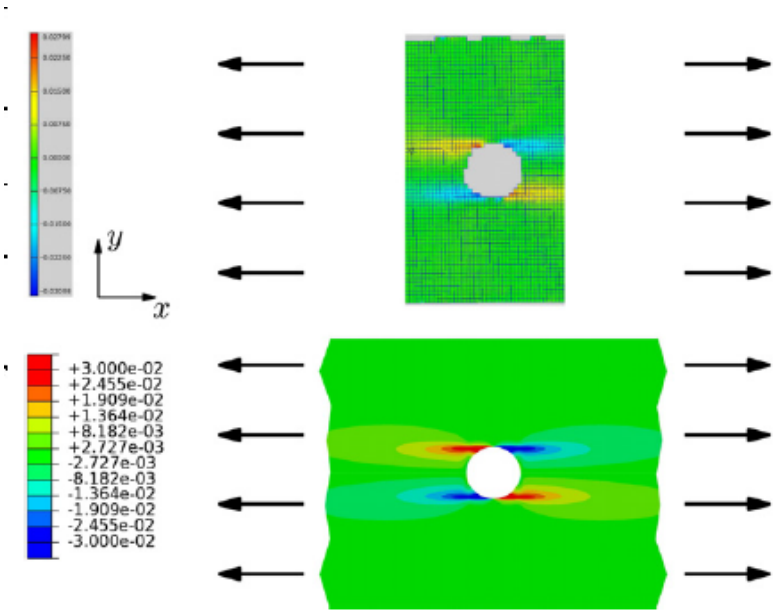

Figure 13: Distribution of laminate shear strain ε_{xy} for part of the $[0/90]_S$ open hole tension test specimen at a load of F=23.6 kN obtained experimentally (top) and at a load of F = 20.9 kN obtained by simulation (bottom), picture taken form [Fla12]

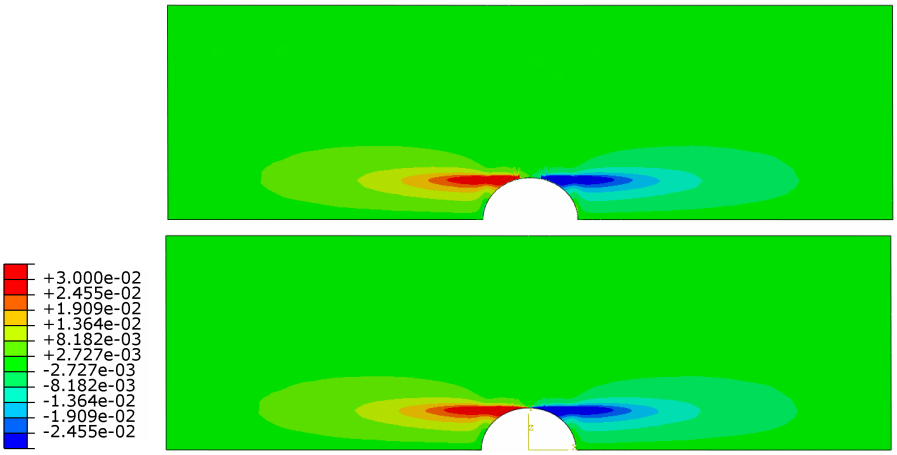

Figure 14: Distribution of ply shear strain ε_{xy} for the $[0/90]_S$ open hole tension test specimen at a load of F=23.8 kN for the 90 degree ply (top) and the 0 degree ply (bottom) obtained by simulation

of the whole (Point A in figure 11) differences occur. These differences are due to two de-lamination zones, to the left and to the right of point A. It can be said that the differences in terms of ply or laminate shear strain are small at this level of the load.
If the distribution of laminate strain in loading direction ε_{xx} is compared, again between the experimentally determined and the results from [Fla12] as well as the results from current thesis, see figure 15 and 16, some differences can be seen. In figure 16 again at the top there is the 90 degree ply and on the bottom is the 0 degree ply with their distributions in laminate strain in loading direction ε_{xx}. Again at the area of point A (see figure 11) the distribution is not equal for both plies due to de-lamination effects. In the 90 degree ply four developing localization zones can be seen. In the experimental results one could be tempted to see similar zones at the top of the whole, non-symmetric but visible. But due to the resolution of the photogrammetric image this can only be speculated.
The figures show results at a load level of 23.6 kN, 20.9 kN and 23.8 kN, respectively. If the load is increased further, the localisation zones as well as the de-lamination zone propagate in direction parallel to the loading direction from the vicinity of the hole towards the clamping area, accompanied by plastic deformation. If the damage accumulation is observed in more detail, it shows four localization patterns in the 90 degree ply, propagating perpendicular to the loading direction. As in the 0 degree ply two damage zone evolve and propagate in loading direction, the damage zones in the 90 degree ply also divert in loading direction. The propagation of the damage zone in loading direction is affected by viscose effects and it cannot be assured that the propagation of this damage zone is not slowed down significantly. In some areas of the fully developed localization zone the volume specific energy dissipated by viscouse effects reaches 60 % of the volume specific energy dissipated by damage. In areas where the damage zone is not fully developed the two energy densities are comparable in value.
At a load level of 36.3 kN, the zone of accumulated matrix damage in terms of the damage variable ξ_2 is shown in figure 17 for the 90 degree ply (top) and the 0 degree ply (bottom). Again differences between both plies occur at the top of the whole, the 90 degree ply shows four separate initial localization zones, whereas the 0 degree ply

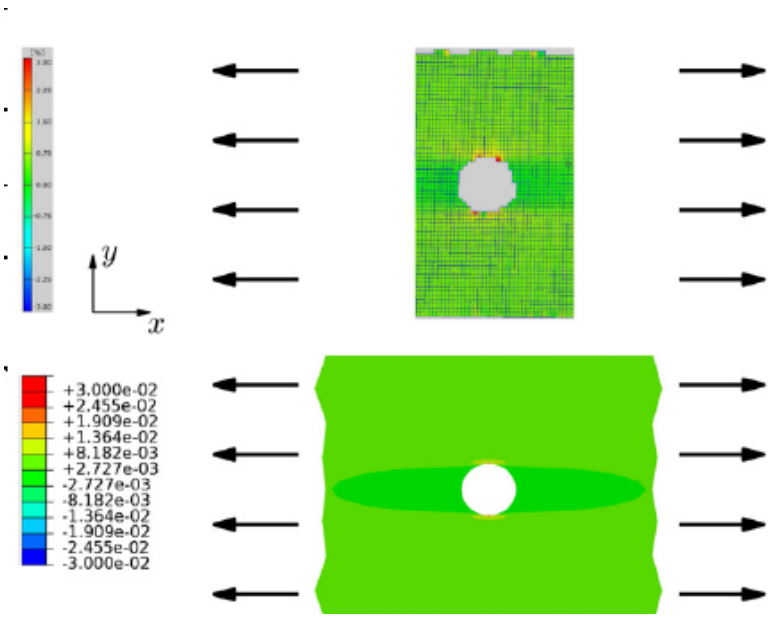

Figure 15: Distribution of laminate strain in loading direction ε_{xx} for part of the $[0/90]_S$ open hole tension test specimen at a load of F=23.6 kN obtained experimentally (top) and at a load of F = 20.9 kN obtained by simulation (bottom), picture taken form [Fla12]

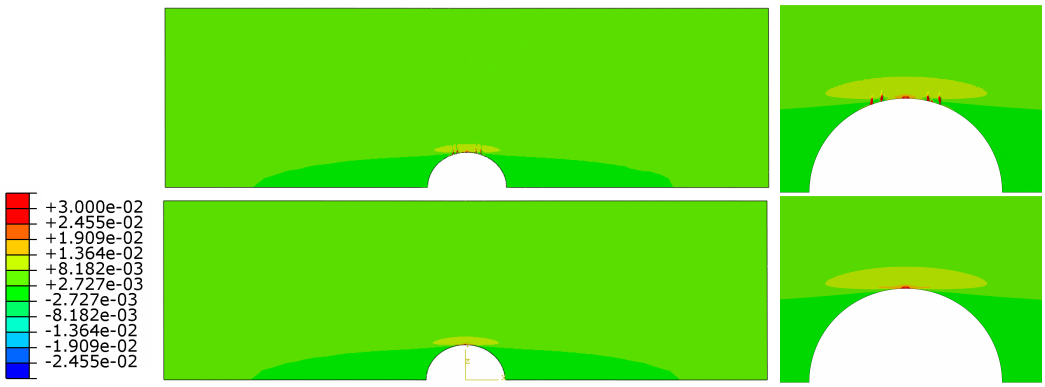

Figure 16: Distribution of laminate strain in loading direction ε_{xx} for the $[0/90]_S$ open hole tension test specimen at a load of F=23.8 kN for the 90 degree ply (top) and the 0 degree ply (bottom) obtained by simulation, view of the whole specimen (left), detailed view (rigth)

only shows two localization zones. Again the differences between both plies suggest de-lamination effects, and also at areas of massive matrix damage de-lamination occurs, see figure 18. The damage pattern predicted can be compared to experimental work, as it was done in [Fla10]. This damage pattern lead to a strongly reduced stress concentration at the vicinity of the whole. This behaviour is shown in figure 19. Here the factor of fibre exertion is shown at $x = 0$ and $y = d/2 \ldots 5d/2$ (line AB in figure 11) for the 0 degree ply at load levels of 23.8 kN (blue line) and 36.3 kN (red line). The blue line is taken at the same load level as figures 16 and 14. This line shows a sharp stress concentration at point A. The red line at a load of 36.3 kN (corresponding to figures 17 and 18) shows a highly reduced stress concentration due to the damage pattern. Care should be taken interpreting the relief of this stress concentration, because the factor of exertion is plotted at the centreline, and two small fibre damage patterns occurred to the left and right, relieving the section in between (figure 17). The 90 degree ply behaves in a similar fashion, the stress concentration is reduced by the development of the damage pattern. At a load level of 36.3 kN nearly the whole 90 degree ply is subjected to damage with a factor of fibre exertion greater than one.

Further rise of the load results in a localization zone perpendicular to the loading direction, propagating from the whole outwards, accompanied by de-lamination. The maximum load is reached at 39,2 kN, where a sharp global snap- back occurs, leading to severe oscillations in the specimen. The global load displacement curve is almost linear until shortly before the maximum load is reached. This maximum load is comparable to [Fla12] (38.4 kN) but overestimates the maximum load reached in the experiments of 25.2 kN. The behaviour at these load levels, meaning the damage of the fibres, is severely affected by viscous effects. Therefore it is questionable whether the predicted peak value is trustworthy. It is possible, that without viscous effects, the localization zone would propagate in a highly dynamic way.

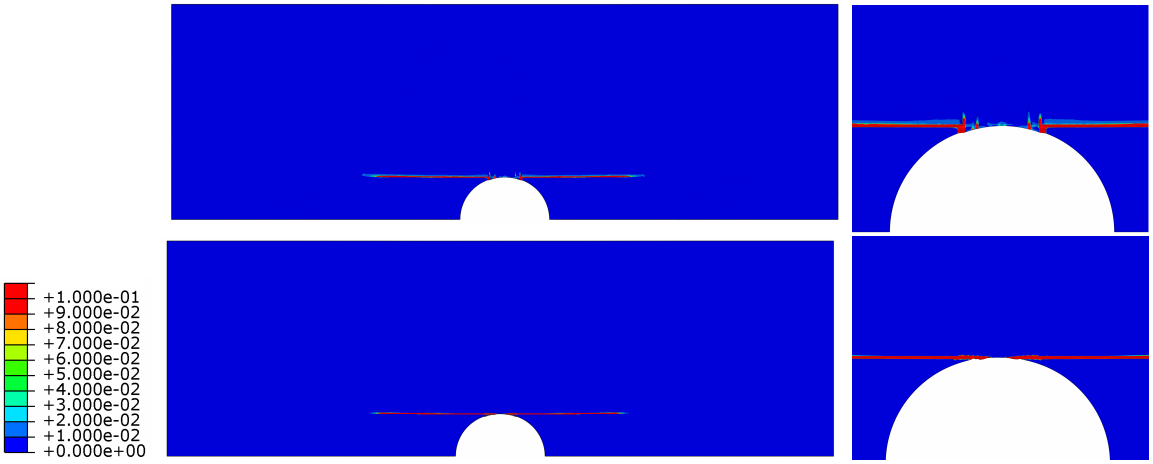

Figure 17: Localization zone in terms of the damage variable ξ_2 for the $[0/90]_S$ open hole tension test specimen at F=36.3 kN for the 90 degree ply (top) and the 0 degree ply (bottom), view of the whole specimen (left), detailed view (rigth)

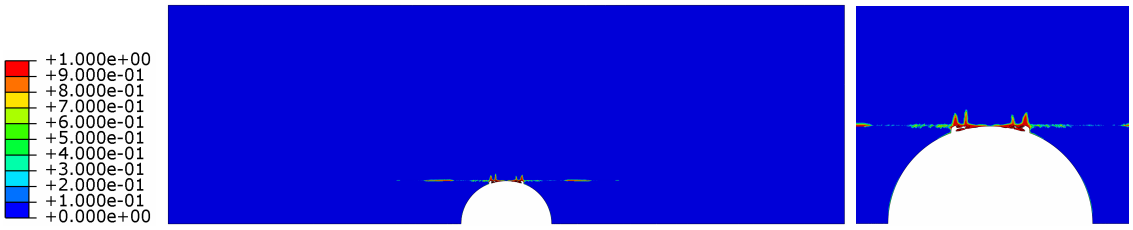

Figure 18: Damage variable of the interface for the $[0/90]_S$ open hole tension test specimen between the 0 degree and the 90 degree ply at F=36.26 kN ,view of the whole specimen (left), detailed view (rigth)

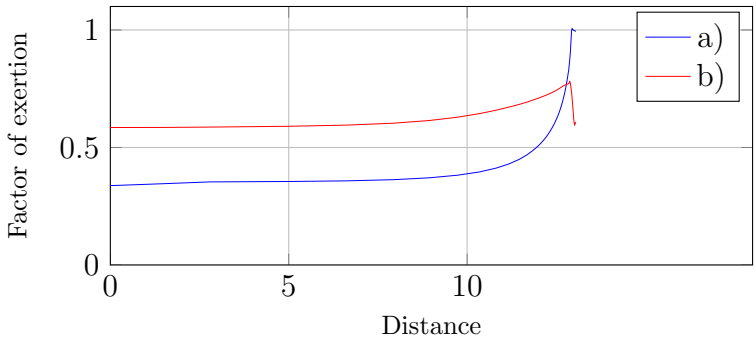

Figure 19: Stress concentration along Line A-B (see figure 11) and its relief for the $[0/90]_S$ *open hole tension test specimen for the 0 degree ply at tensile loads of 23.8 kN (a) and 36.3 kN (b) in terms of the factor of fibre exertion*

Results for layup $[-45/+45]_S$

The second layup under consideration is a $[-45/+45]_S$ laminate. In this layup, no fibres are oriented in loading direction, the overall stiffness is lower as in the above $[0/90]_S$ laminate. This results in longer calculation times of about 30.5 hours (on a standard desktop Pc) due to the limits in load rate scaling. As the structural response is greatly non-linear this also enlarges the calculation time due to the changes in the structural stiffness. The FEM mesh of the current specimen is shown in figure 20, again at the vicinity of the whole an element length of 0.03 mm is used, the localization zones extends in a x-shaped area, where the mesh size is held approximately constant.

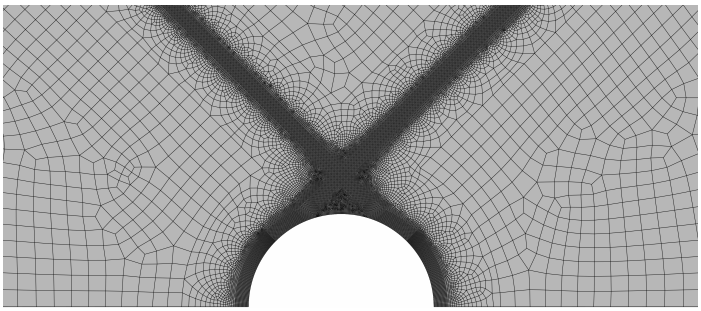

Figure 20: Detail view of the mesh of the $[+45/-45]_S$ *open hole tension test specimen*

The non-linearity prior to damage initiation is mainly due to the accumulation of unrecoverable strains, namely plastic shear strains $\gamma_{12}^{(\mathrm{pl})}$. The first occurrence of plasticity is observed at a relatively low load level of 1.5 kN at the vicinity of the hole. The

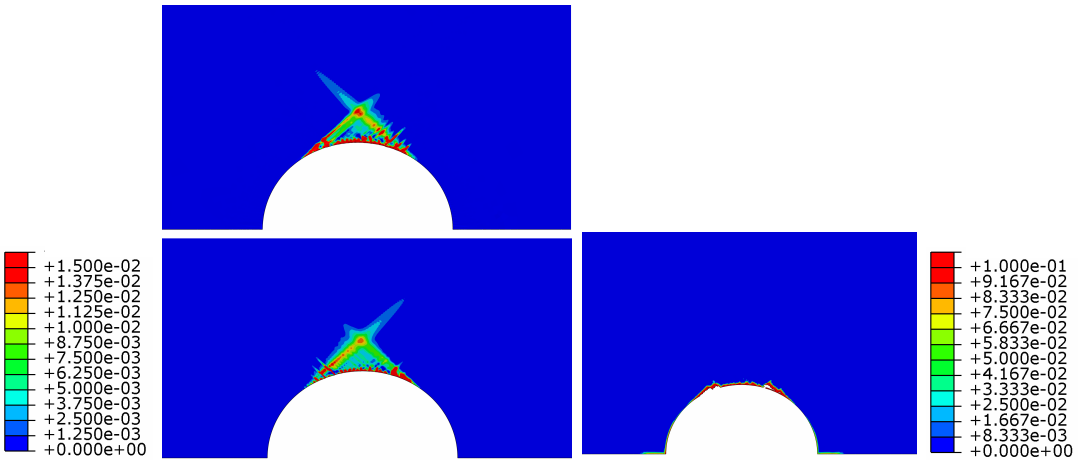

Figure 21: Localization zone in terms of the damage variable ξ_2 for the $[-45/+45]_S$ open hole tension test specimen for the +45 degree ply (top) and the -45 degree ply (bottom) at a load of F=8.6 kN (left) and damage variable of the interface between the -45 degree and the +45 degree ply at a load of F=8.6 kN (right), obtained by simulation, partial view of the specimen

area affected by plasticity spreads and covers nearly the whole specimen at a load of 3 kN with peak values near point A, at the top of the hole. Further raise of the load level leads to further accumulation of plastic shear strains with the initiation of damage at a load of 4.6 kN to the right of point A for the -45 degree ply and the left of point A for the +45 degree ply, accompanied by first occurrence of interface damage. The matrix damage patterns extend in radial direction with first signs of damage localization at a load of 6.7 kN. Some five to ten individual localization zones can be observed in each ply, again to right of point A for the -45 degree ply and to the left of point A for the +45 degree ply. As the load is increased more small localization areas occur, some of them keep growing, accompanied by interface damage. Shown in figure 21 is the distribution of matrix damage variable ξ_2 for both plies (left) and the corresponding damage variable of the interface (right) at a load of 8.6 kN, . The maximum value of the scale is set to the point of localization onset. Here one can see the evolution of localization zones parallel to the fibre direction for both plies. After Onset of localization, the damage patterns will form the known damage pattern. At this load level of 8.6 kN, just before the formation of the major localization patterns, the simulations are compared to the measurements and simulations of [Fla12]. Here it

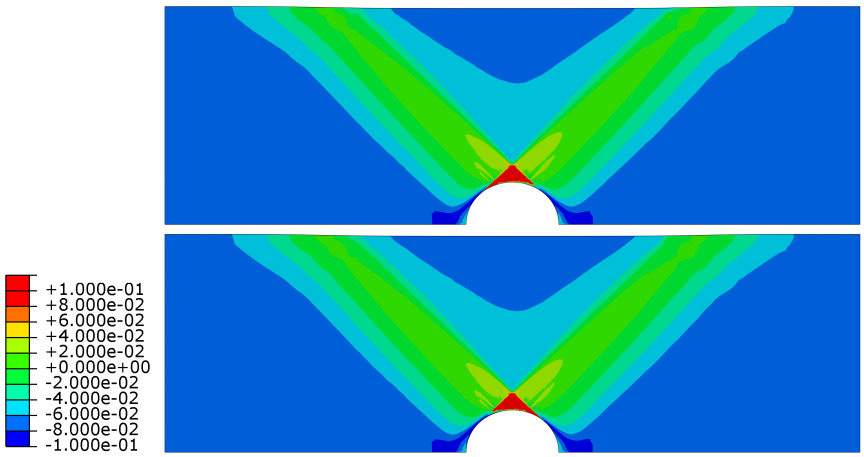

Figure 22: Distribution of accumulated plastic matrix shear strain γ_{12} for the $[-45/+45]_S$ open hole tension test specimen for the +45 degree ply (top) and the -45 degree ply (bottom) predicted by FEM simulation at a load of 8.6 kN, the interface is not shown

has to be mentioned, that in the current simulations the initiation of damage occurs at lower load levels than in the simulations of Flatscher. The distribution of accumulated matrix shear strain γ_{12} is shown in figure 22. The distribution of laminate strain in loading direction ε_{xx} and in transverse direction ε_{yy} from the work of Flatscher are shown in figures 23 and 25 and from the current work in figures 24 and 26. The results in terms of ε_{xx} and ε_{yy} do not agree as well with the measured strain fields as in the original work, because the initiation and evolution of damage is predicted at lower load levels. This behaviour also leads to smaller maximum loads. At the peak load of 9 kN the damage pattern of the plies and the interace is shown in figure 27. Clearly visible is the asymmetric development of the ply damage localization zone. The peak load of 9.0 kN is lower as the measured peak load of 14.1 kN and is also lower as the peak load of the simulation of Flatscher of 10.7 kN. This underestimation of the structural strength may be explained by the considerable shear strain which exceed the small strain assumption. Another reason can be the estimated damage behaviour of the interface. It can be suggested that important mechanisms are captured well by the current material model in conjunction with the applied approach of simulating the plies individually with interfaces in between.

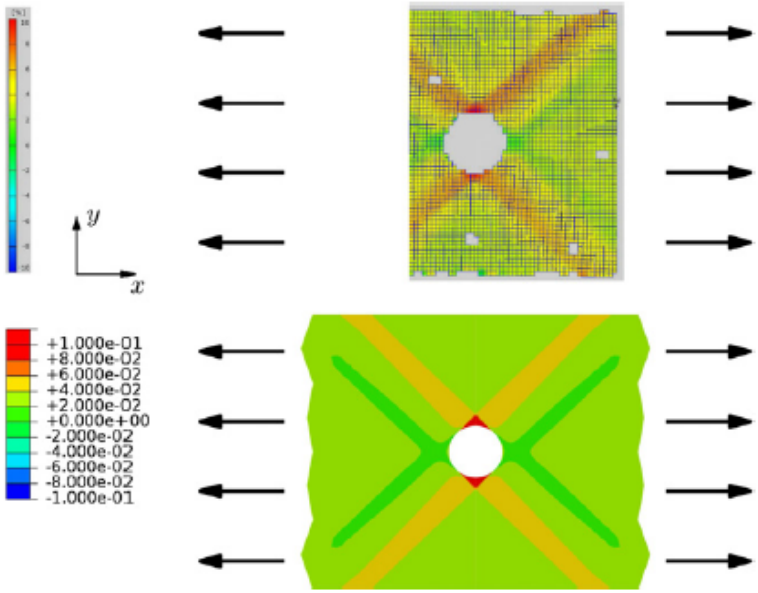

Figure 23: Distribution of laminate strain in loading direction ε_{xx} for the $[-45/+45]_S$ open hole tension test specimen at a load of F=10.6 kN obtained experimentally (top) and at a load of F = 9.8 kN obtained by simulation (bottom), picture taken from [Fla12]

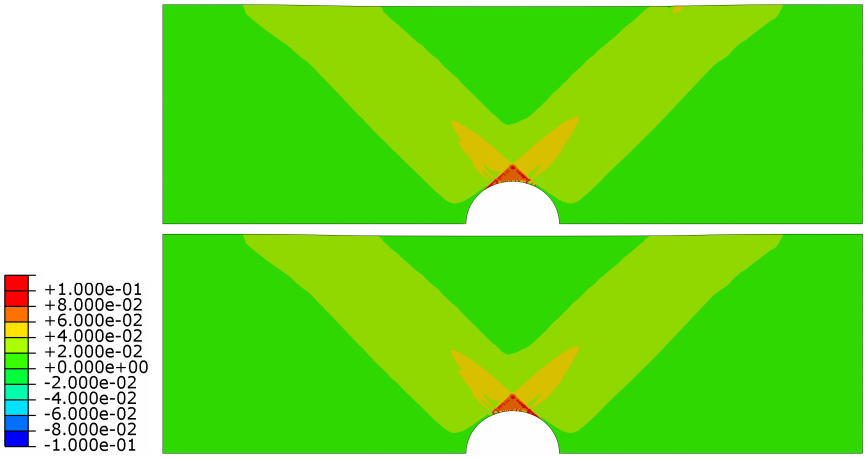

Figure 24: Distribution of laminate strain in loading direction ε_{xx} for the $[-45/+45]_S$ open hole tension test specimen at a load of F=8.6 kN for the +45 degree ply (top) and the -45 degree ply (bottom), obtained by simulation

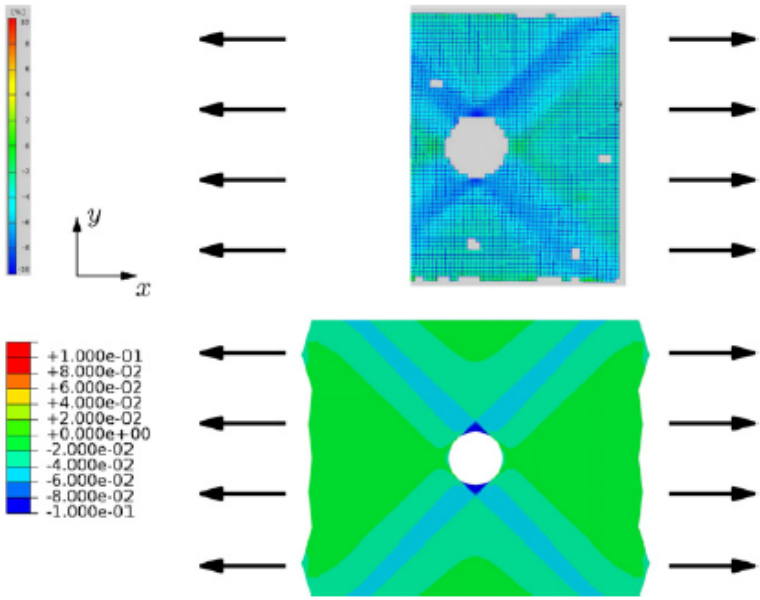

Figure 25: Distribution of laminate strain in transverse direction ε_{yy} for the $[-45/+45]_S$ open hole tension test specimen at a load of F=10.6 kN obtained experimentally (top) and at a load of F = 9.8 kN obtained by simulation (bottom), picture taken from [Fla12]

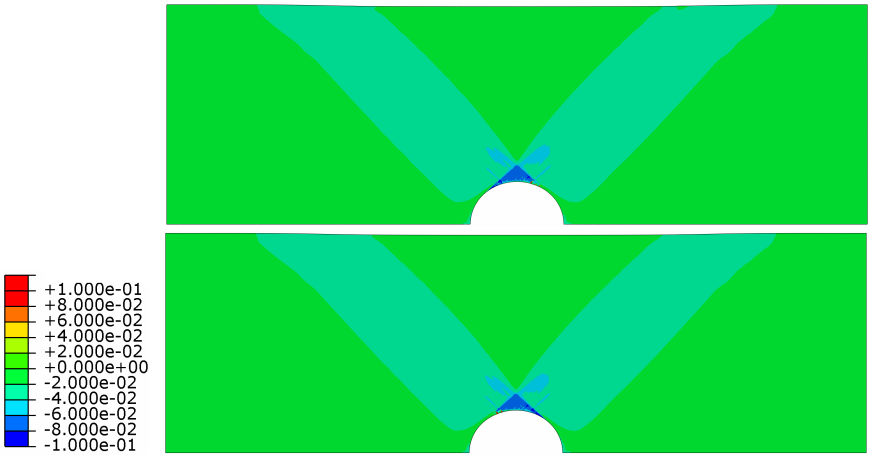

Figure 26: Distribution of laminate strain in transverse direction ε_{yy} for the $[-45/+45]_S$ open hole tension test specimen at a load of F=8.6 kN for the +45 degree ply (top) and the -45 degree ply (bottom), obtained by simulation

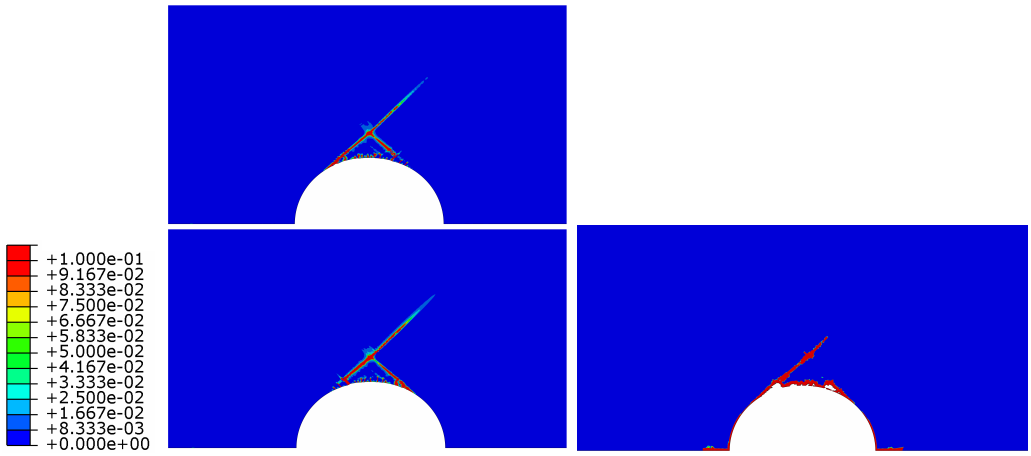

Figure 27: Localization zone in terms of the damage variable ξ_2 for the $[-45/+45]_S$ open hole tension test specimen for the +45 degree ply (top) and the -45 degree ply (bottom) at a load of F=9.0 kN (left) and Damage variable of the interface between the -45 degree and the +45 degree ply at F=9.0 kN (right), obtained by simulation, partial view of the specimen

Results for layup $[0/-45/90/+45]_S$

The last open hole specimen under consideration is a layup of $[0/-45/90/+45]_S$. This sometimes called quasi-isotropic layup is relatively stiff, leading to a rather short calculation time of 8.5 hours. In figure 28 the mesh is shown. In this simulation the mesh is chosen relatively coarse with an element length of approximately 0.05 mm at the vicinity of the whole. This is done due to the number of plies. In the two simulations above two plies and one interface have been modelled, whereas here the four plies and three interfaces modelled lead to a high number of degrees of freedom. The mesh is chosen the same for all plies and interfaces. For this layup of the open hole specimen no experimentally measured strain fields are available. Therefore the results of the simulation is shown on its own. The global load displacement behaviour is nearly linear, although the simulation shows highly non-linear behaviour of the single plies and interfaces. The first occurrence of interface damage is at a load of only 2.5 kN, restricted to a very small area at the vicinity of the whole. At a load level of 4.5 kN the damage of the interface has grown insignificantly, first signs of plasticity are observable for the 0 degree, +45 degree and −45 degree ply. First distributed brittle damage accumulation starts at a load of 10.8 kN, at the −45 degree and 90 degree ply.

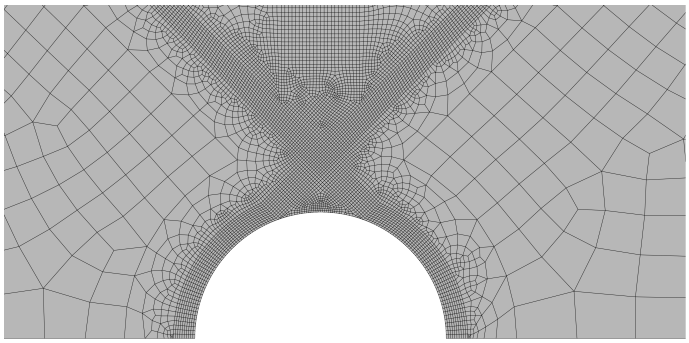

Figure 28: Detail view of the mesh of the $[0/-45/90/+45]_S$ *open hole tension test specimen*

Now signs of plasticity are observable at all plies. At a load level of 17.0 kN the +45 degree and the -45 degree ply are nearly completely affected by plasticity. Damage localization started not just yet in the -45 degree ply, first signs of fibre damage are observable in the 0 degree ply. All in all it can be said, that the damage patterns are similar to the damage patterns evolved in the $[0/90]_S$ and $[+45/-45]_S$ prior to localization. In figure 29 the distribution of laminate strain in loading direction ε_{xx} is shown for the four plies at a load of 17.0 kN. At the vicinity of the hole the maxima are shifted to the left and right due to de-lamination. The de-lamination effects are restricted to a small area around the whole, shown in figure 30. If one looks at the distribution of laminate shear strain ε_{xy}, see figure 31, one can see a similar pattern in the 0 degree ply as it occurs in the $[0/90]_S$ specimen. The distribution differs between the plies, suggesting that an influence of the stacking sequence is observable.

The pattern of accumulated plastic shear strains in the 0 degree ply is nearly equal in shape as for the 0 degree ply in the $[0/90]_S$ specimen (not shown in this thesis). Increasing the load leads to damage localization first in the -45 degree ply, followed by the 90 degree, the +45 degree and the 0 degree ply. The evolution of these damage patterns leads to the complete failure of the specimen. At the peak load of 32.0 kN the matrix damage pattern is shown in figure 32. The 0 degree ply exhibits combined matrix and fibre damage in a zone perpendicular to the loading direction. This developing damage zone limits the load carrying capacity of this specimen. But at this time the influence of viscous regularization is already big, meaning the volume specific energy

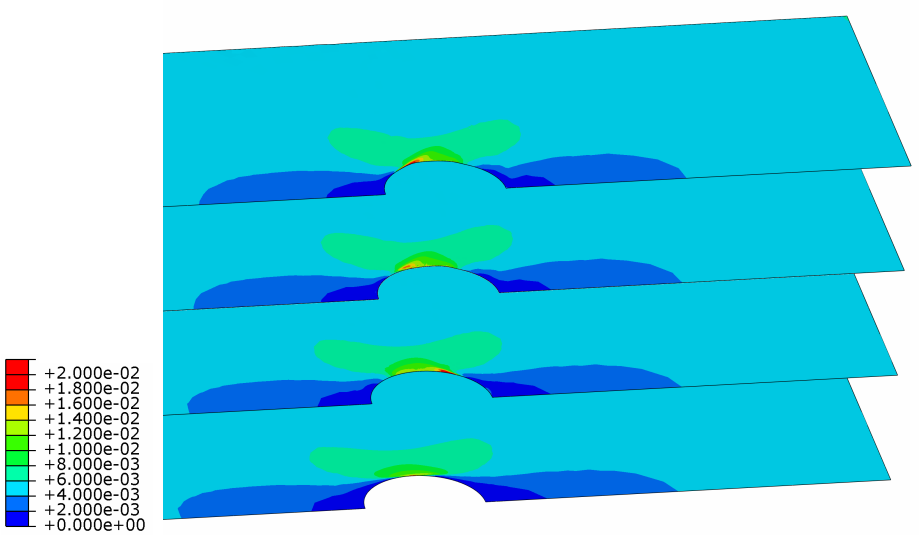

Figure 29: Distribution of laminate strain in loading direction ε_{xx} for part of the $[0/-45/90/+45]_S$ open hole tension test specimen at a load of F=17.0 kN obtained by simulation, z direction is enlarged for better visibility, plies from bottom to top: 0/-45/90/+45

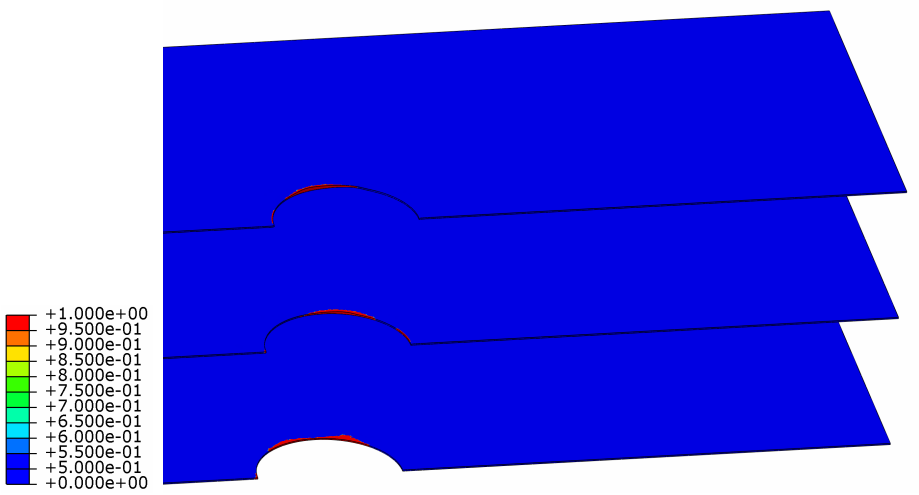

Figure 30: Distribution of interface damage for part of the $[0/-45/90/+45]_S$ open hole tension test specimen at a load of F=17.0 kN obtained by simulation, z direction is enlarged for better visibility, interfaces from bottom to top: 0/-45, -45/90, 90/+45

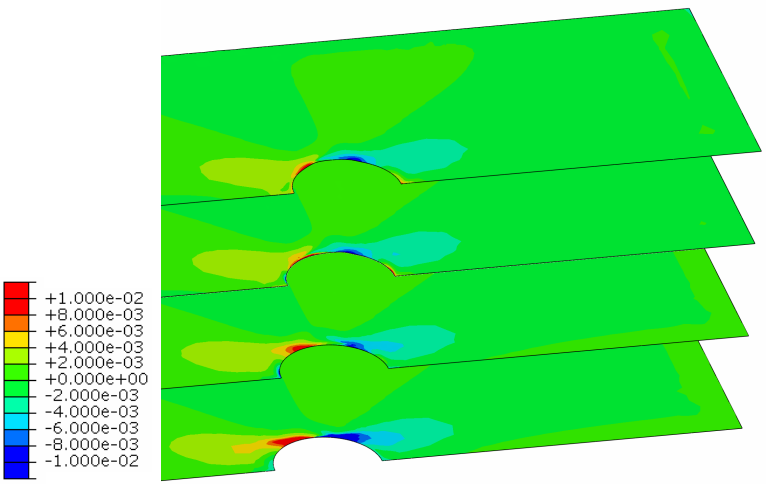

Figure 31: Distribution of laminate shear strain ε_{xy} for part of the $[0/-45/90/+45]_S$ open hole tension test specimen at a load of F=17.0 kN obtained by simulation, z direction is enlarged for better visibility, plies from bottom to top: 0/-45/90/+45

dissipated through viscous regularization is at half the value of the volume specific energy dissipated by damage, in most of this localization areas. Therefore it is possible, that the peak load is overestimated in this simulation. The +45 degree ply behaves as expected, a localization zone in fibre direction evolves. The interfaces between the plies are at this load level damaged in wide areas, see figure 33.

Due to this de-lamination areas, the damage behaviour of the individual plies is not coupled any more allowing for individually evolving localization patterns. The displacement of part of the 90 degree and + 45 degree plies in out of plane direction at the vicinity of the whole can be explained by these de-laminated areas and dynamic influences.

The prediction given by this simulation is not compared to any test data, as no such data was found in the literature. The damage patterns beyond maximum load are not showed, because the specimen might behave highly dynamic as it is highly influenced by viscose regularization.

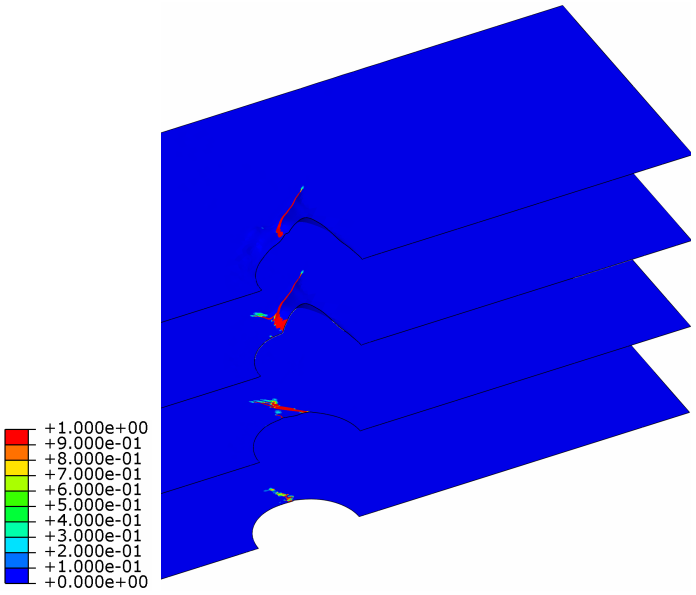

Figure 32: Localization zone in terms of the damage variable ξ_2 for part of the $[0/-45/90/+45]_S$ open hole tension test specimen at F=32.0 kN obtained by simulation, z direction is enlarged for better visibility, plies from bottom to top: 0/-45/90/+45

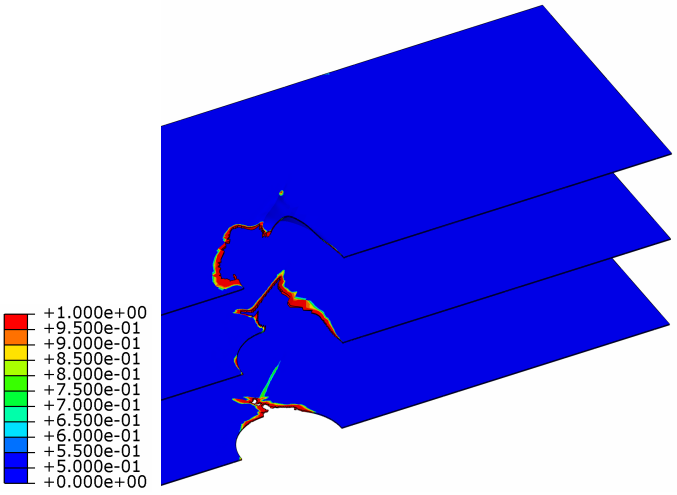

Figure 33: Distribution of interface damage for part of the $[0/-45/90/+45]_S$ open hole tension test specimen at a load of F=32.0 kN obtained by simulation, z direction is enlarged for better visibility, interfaces from bottom to top: 0/-45, -45/90, 90/+45

5.4 Unit cell

To investigate the potential concerning the numerical stability, computational efficiency as well as the low requirements to the computer hardware, a simulation of an unit cell was carried out. This Unit Cell is a part of Jakob Gager's Ph.D. [Gag13], which investigates the mechanical response of braided and woven composites in the framework of the FEM. His modelling approach is based on homogenization of periodic unit cells. To this end he has developed an unit cell discretized by shell type Finite Elements. Some of the simulations were conducted with the EDP constitutive law from Flatscher [Fla10]. So it is an obvious choice for a comparison between the two implementations of the EPD-model with Abaqus/Standard and -/Explicit.

A sketch of an Unit Cell can be seen in figure 34, with its coordinate systems, and a sketch of the tow and matrix geometry in figure 35, taken from [Gag13].

The use of Unit Cells assumes a periodic meso-structure, meaning the Unit Cell can be

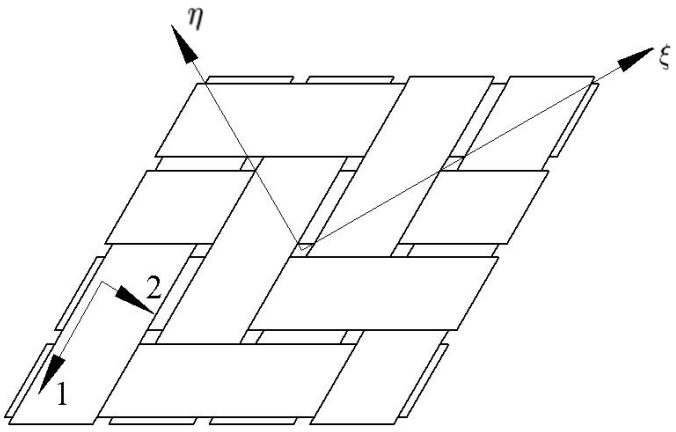

Figure 34: Sketch of a 2/2 twill weave ±30 unit cell shown without matrix material and the coordinate systems $\xi - \eta - \zeta$ and $1 - 2 - 3$ (local tow), after [Gag13]

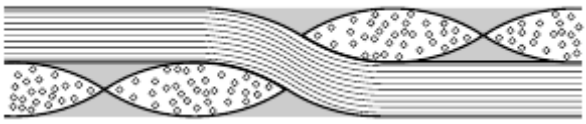

Figure 35: Sketch of the idealized tow and matrix geometry of a 2/2 twill weave, matrix indicated in grey, picture taken from [Gag13]

arranged periodically to make up the macroscopic woven ply material. To assure this periodicity, special boundary conditions have to be applied. This boundary conditions have to assure compatible deformations at corresponding edges of the unit cell at all times. So called master nodes are used to describe the mean deformation of the Unit Cell with respect to macroscopic stresses and strain, respectively, as done by [Pah03]. This master nodes are located at the corners of the Unit Cell, and, by the way the boundary conditions are implemented, they can be used to apply appropriate forces and displacements, respectively. The master nodes are also used to derive the effective stresses and strains.
Two constitutive laws are applied in the Unit Cells. The EPD model is used for the tows (the bundles of fibres) and the regions of 'pure' resign material are described by an isotropic elastic material behaviour. An attempt was made to use a Drucker-Prager type plasticity model for the regions of 'pure' resign material, as typically used for polymers, in an explicit simulation as this was not possible in the implicit one.

In the current thesis one of the Unit Cells developed and implemented by Jakob Gager is used to compare the implicit and explicit FEM. The choice falls on a 2/2 Twill weave with an angle of ± 30 degree , which is a strain free skewed, single layered, orthogonal (± 45 degree) Unit Cell with lenticular cross section of the tows. This Unit Cell is subjected to an uni-axial load in braiding direction, meaning uniaxial tension in ξ direction. The material system in use is RTM6/HTS40, the material parameters can be found in [Gag13]. The matrix pockets exhibit linear elastic behaviour and all interfaces are assumed to be perfect. The results of the explicit and implicit FEM simulations conducted with the original model from Gager and the explicit model based on Gagers work agree in wide areas. The distribution of accumulated plastic shear strain γ_{12} in the tows is shown in figure 36, the matrix material is hidden for better visibility. Both plots are taken at the same load level before damage localization occurs. At higher loads damage starts to localize, first at the intersections of the individual tows, followed by a localization pattern within the tows. But as periodic boundary conditions are applied, it is questionable whether the solutions at this load level is trustworthy,

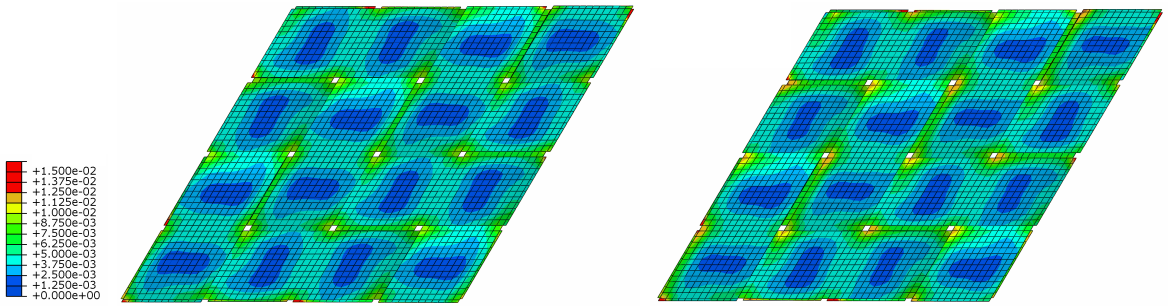

Figure 36: Distribution of accumulated plastic shear strain γ_{12} at the top of the ± 30 degree unit cell shown without matrix material, from the implicit simulation of Gager [Gag13] (left) and the explicit simulation based on Gager's model (right); the contour limits are the same for both plots, taken at the same load level

due to the damage localization. Another problem arises at high loads, the elements at the boundary (the edge elements) start to take too much damage, resulting in heavily distorted elements. Therefore only the distribution of the damage variable ξ_2 at an intermediate load level, before the localization pattern within the tows occurs, is plotted in figure 37, again for the explicit and implicit FEM simulations.

If the material of the matrix pockets is described by an elasto-plasto Drucker-Prager material model, the explicit solution is not notably affected up to the point of strain localization. Beyond this load level the edge elements start to distort earlier and the explicit simulation has to be stopped. The solutions are not shown here, because they are judged not trustworthy.

Two problems arise in the explicit simulation. The first problem concerns the material

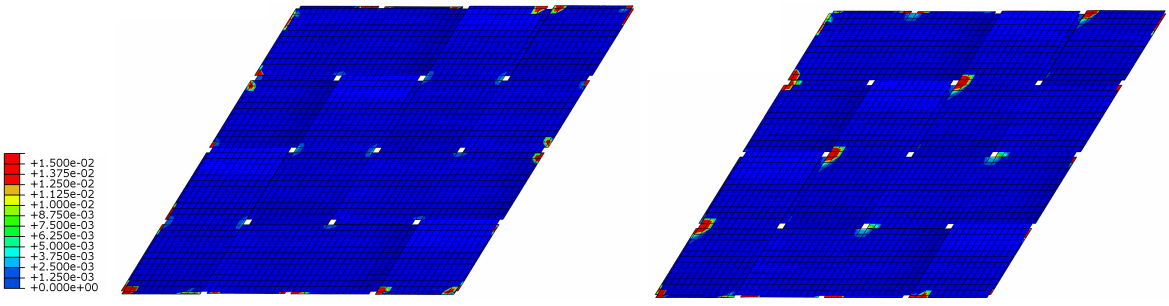

Figure 37: Distribution of the damage variable ξ_2 at the top of the ± 30 degree unit cell shown without matrix material, from the implicit simulation of Gager [Gag13] (left) and the explicit simulation based on Gager's model (right); the contour limits are the same for both plots, taken at the same load level

model itself, in the user subroutine occur convergence problems at Level 2 (see chapter 3.4 Implementation). The predictor-corrector algorithm used to iteratively solve the combined plasticity and damage state has convergence problems, resulting in the attempt to reduce the load (time) increment, as it is done in the implicit simulation. As this is not possible in the framework of Abaqus/Explicit, the simulation should be stopped. The time increment necessary for the user subroutine to converge is too small for a decent calculation time and also the user time needed would not be reasonable. A rather bold approach is chosen, meaning the the simulation is continued even though convergence is not achieved in a few of the elements. This resulted in a rather short calculation time of only 30 hours on one cpu, compared to 24 hours with the implicit solver and four cpu's. The drawback can be seen by the differences in figure 37, although the global stress strain relation is only approximately 3% off. The requirements in memory are comparable for both simulations, due to the relatively low number of elements. The second alteration concerns the warping of the Unit Cell. The implicit simulation followed the trivial path, whereas in the explicit simulation the solution showed signs of warping. To avoid this behaviour as it would not occur in nature due to the stacking of the plies, appropriate boundary conditions have been applied to the master nodes. These boundary conditions disabled the possibility of multi processor operations. This disables one major advantage of the explicit integration scheme. Without multi processor operations one has to compare a calculation time of 30 hours with the explicit simulation to the inplicit simulation which took only 24 hours to complete.

Finally, one has to say that there is no advantage in using Abaqus/Explicit for this particular problem, although the solutions could be reproduced. The calculation time and memory required are comparable for both simulations, but the accuracy is lower in the explicit one. Also it was not possible to incorporate plasticity in the matrix pockets, which would give an advantage over the implicit simulation.

6 Potential extension

The goal specified at the beginning of the thesis, the adaptation of Flatscher's EDP model to Abaqus/Explicit, was reached. The mechanical response in the implicit and explicit FEM agree with within the tolerances needed. The handling of the EDP-model in conjunction with Abaqus/Explicit differ in some details from the original implementation, but for an operator familiar with the original implementation and its constitutive behaviour this will not be of great concern. Nevertheless there are some topics still in question and possible investigations of interest.

- As the EDP model was incorporated without changes in its behaviour its limitations are still valid. It is applicable for plane stress, small strain problems.
- As the simulations conducted in this thesis are all of quasi-static nature it was decided to leave the possible influence of the viscous regularisation untouched. This was done to assure comparability between the implicit and explicit simulations. If dynamic problems are to be simulated, this viscous influences should be investigated thoroughly.
- As Abaqus/Explicit offers the possibility of element deletion, it would be of interest to incorporate this behaviour for simulations where areas of severe ply damage occurs, as it may lead to convergence problems. Element deletion would be quite easy to implement in the user subroutine, the clue is to find a proper condition to do so.
- In Abaqus it would be possible to combine both Integration methods, the implicit and the explicit one. It should lead to shortened calculation times if the linear part of the analysis is conducted with an implicit simulation, and the non-linear part is then restarted and finished with the explicit integration scheme.
- Furthermore, it would be of great interest to investigate the influence of the stacking sequence. This would be possible with the approach chosen, the combination of shell elements for the ply and cohesive elements for the interface, but was not carried out.

7 Summary

With the increasing use of FRP's in industries the need of a reliable simulation technique is immanent. Such reliable simulation methods, for example the FEM, call for a robust solution method capable of capturing the linear as well as the non-linear mechanical behaviour of structures. To this end the Elasto-Plasto-Damage-Constitutive law from [Fla10] was adapted to be used in conjunction with the explicit FEM package Abaqus/Explicit. An user subroutine is written to adapt the given EPD-model to Abaqus/Explicit and it is verified. This EDP-model is capable to describe the combined Elasto-Plasto-Damage behaviour of uni-directional reinforced Laminates. To go one step further, this EDP-model was combined with so called cohesive elements to capture the interface behaviour between the plies, possibly influenced by damage. This lead to the current approach, where the plies are modelled individually with an interface layer in between. This approach enables the investigation of the individual plies and interfaces and their damage (and plasticity) behaviour, giving insight in the specimens. Three types of simulations are carried out. A simulation of a three point bending specimen, showing the interrelation of distributed brittle matrix damage and localized brittle matrix damage. Open hole tension tests are simulated to show the capability to describe the combined plasticity and damage behaviour of the individual plies, as well as the behaviour of the interfaces. The third application is an unit cell of a braided composite to investigate the numerical stability as well as the calculation time required.

Finally one can describe the chosen approach in conjunction with the explicit integration scheme as very promising. The simulations show a good agreement with experiments, see [Fla12] although in some cases deviations exits. The numerical stability as well as the numerical efficiency for big systems is a major advantage in comparison to the implicit FEM.

References

[Par66] Heinz Parkus (1966): *Mechanik der festen Körper, unveränderter Nachdruck 2005*. Springer Verlag, Wien

[Aba10] Dassault Systemes (2010): *Abaqus Analysis User's Manual*. Velizy-Villacoubblay, Frankreich

[Aba11] Dassault Systemes (2010): *Abaqus Verification Manual* . Velizy-Villacoubblay, Frankreich

[Aba12] Dassault Systemes (2012): *Abaqus User Subroutines Reference Manual*. Velizy-Villacoubblay, Frankreich

[Fla10] Thomas Flatscher (2010): *A Constitutive Model for the Elasto-Plasto-Damage Ply Behavior in Laminated FRP Composites: Its Developement, Implementation and Application in FEM Simulations*. VDI Verlag, Duesseldorf

[Bat02] Klaus-Juergen Bathe (2002): *Finite-Elemente-Methoden*. Springer Verlag, Berlin-Heidelberg

[Nas10] Lutz Nasdala (2010): *FEM-Formelsammlung Statik und Dynamik*. Vieweg+Teubner, Wiesbaden

[Puc96] Alfred Puck (1996): *Festigkeitsnanalyse von Faser-Matrix-Laminaten*. Carl Hanser Verlag, Munchen Wien

[Fla12] Thomas Flatscher, Markus Wohlfahrt, Gerald Pinter, Heinz Pettermann (2011): *Simulations and experiments of open hole tension tests - Assessment of intra-ply plasticity, damage and localization*. Composite Science and Technology, 72, p. 1090-1095, Elsevier

[Fla13] Thomas Flatscher, C. Schuecker, H.E. Pettermann (2013): *A constitutive ply model for stiffness degradation and plastic strain accumulation: Its*

application to the Third World Wide Failure Exercise (Part A). Journal of Composite Materials, 47, p. 4575-2593

[Pah03] Dieter Pahr (2003): *Experimental and Numerical Investigations of Perforated FRP-Laminates.* VDI Verlag, Duesseldorf

[Bau03] Wolfgang Baumann, Christian Boehning (2003): *Einfuehrung in die Programiersprache FORTRAN 77.* Herrmann-Foettinger-Institut fuer Stroemungsmechanik,Technische Universitaet Berlin

[Dun05] Fionn Dunne, Nik Petrinic (2005): *Introduction to Computational Plasticity.* Oxford University Press, New York

[Har06] F. J. Harewood, P.E. McHugh (2006): *Comparison of the implicit and explicit finite elelemt methods using cristal plasticity.* Education and Research Promotion Program (2009), Korea University of Technology and Education

[Yan11] Yang, Seung-Yong (2011): *Conversion of Abaqus user Material Subroutines.* Journal of the Computational Structural Engineering Institute of Korea, 23, p. 635-640

[Hal09] S. R. Hallett, B. G. Green, W. G. Jiang, K. H. Cheung, M. R. Wisnom (2009): *The open hole tension test: a challenge for virtual testing of composites..* International Journal of Fracture,158(2), p 169-181

[Gag13] Jakob Gager (2013): *Modeling and simulation concepts for advanced braided composites.* PhD thesis, Institute of Lightweight Design and Structural Biomechanics, Vienna Univerity of Technology, Vienna, Austria

[Sch05] Clara Schuecker (2005): *Mechanism based modeling of damage and failure in fiber reinforced polymer laminates.*PhD thesis, Institute of Lightweight Design and Structural Biomechanics, Vienna Univerity of Technology, Vienna, Austria

A Usage of the Vumat

The usage of the current Vumat differs only by some minor details from the usage of Flatscher's Umat. As it is not suggested to use the current Vumat without detailed knowledge of Flatscher's Umat, only the differences are described.

Material input

In this thesis two sets of material parameters are used, namely Cycom977 and IRTM6/ HTS40. The complete set of material parameters can be taken from Flatscher [Fla10] or Gager [Gag13].

If a new material-input has to be created, the reader is refereed to the original thesis by Flatscher [Fla10]. From the Input of the Umat only a few alterations have to be made. These alterations are:

- The number of solution dependent variables (SDV) is raised to 350 and is set in conjunction with the keyword *DEPVAR.
- It is advised to set the switch concerning the Output (PROPS(3)) to zero.
- The viscous parameters (PROPS(45 ... 48)) have to be scaled according to the loading rate.
- If initial conditions are used for the SDV's, ten entries have to be added to account for their raised number. These entries have to be set to zero.
- The procedure to account for the roughly estimated stable time increment has to be re-evaluated.

Output

The Output remained unchanged except for SDV(14) and SDV(15), they have no meaning any more. The Output written to 'file' (meaning the .msg file) is impractical in use with Abaqus/Explicit, therefore it was eliminated. The only possibility to check

the solution if non-severe errors occurred during the simulation is to monitor SDV(4) and SDV(16) throughout the analysis. If errors occur, they are written to SDV(16) as integers. In table A1 and A2 these integers are explained, taken directly from the Fortran code of [Fla10].

Table A1: Non-severe error code for SDV(16), taken from [Fla10]

-1)	ERROR:UMAT: FT SOFT WITH TOO COARSE MESH
-2)	ERROR:UMAT: FC SOFT WITH TOO COARSE MESH
-3)	ERROR:UMAT: MT SOFT WITH TOO COARSE MESH
-4)	ERROR:UMAT: MC SOFT WITH TOO COARSE MESH
-5)	ERROR:KXFSOF: FIBER SOFTENING PROHIBITED
-6)	ERROR:KXMSOF: MATRIX SOFTENING PROHIBITED
-17)	ERROR:KPRESO: PIECEWISE NOT IMPLEMENTED
-27)	ERROR:KHARD: INCORRECT TABLE
-35)	ERROR:UMAT: BAD WEAKENING PARS
-38)	ERROR:UMAT: FIBER EXERTION > 1
-39)	ERROR:UMAT: MATRIX DAMAGE AMOUNT > XIMC
-40)	ERROR:UMAT: MATRIX EXERTION > 1

Stable time increment

The estimation of the stable time increment $\Delta t'_{\text{stable}}$ in conjunction with the Vumat is not as accurate as expected. It turns out that (for the material cycom977) the stable time increment is overestimated, depending on the fibre orientation angle ψ, see figure 1. This behaviour is shown in figure A1, in terms of estimated stable time increment $\Delta t'_{\text{stable}}$ over the fibre orientation angle ψ for $\psi = \pm 90°$, as it repeats itself. This may lead to numerical instabilities if no measures are taken. One possibility to handle this behaviour is to scale the time increment globally, for example with the option *scale factor. But this may lead to an increase in calculation time by a factor of maximal 3.2, which is especially unsuited for quasi-static analyses, as for this kind of analyses it is mostly suitable to use a time increment shortly smaller as the stable time increment. For quasi-static analyses the use of mass scaling is mostly desired. As this option depends on the estimated stable time increment, problems arise. The density of single elements is only risen if the estimated stable time increment is below a certain value given. Due to the error in estimating the stable time increment this leads to insufficient distribution of added mass. If areas of similar orientated fibres can be found the option mass scaling can be used by assigning different values of the stable time increment desired. If for example the desired stable time increment for a fibre orientation angle of $psi = 45°$ is set to $2 * 3,2 \cdot 10^{-8}$ and for $\psi = 0°$ it is set to $2 * 1,4 \cdot 10^{-8}$ the mass added will be approximately the same. This procedure does not prevent problems with instabilities, but helps to minimize them.

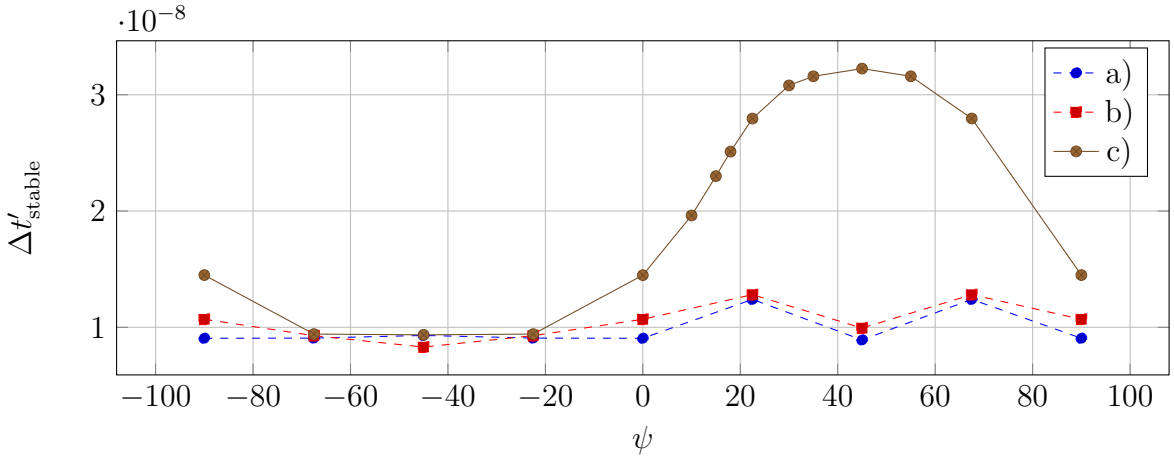

*Figure A1: Example of the estimated stable time increment $\Delta t'_{stable}$ as a function of the fibre orientation angle ψ in degrees for a quadratic shell element (S4R), a) for the built in Material *Elastic,Type=Lamina, b) for the built in Material *Elastic,Type=Engineering Constants and c) in use with the user Subroutine*

Table A2: Severe error code for SDV(16), taken from [Fla10]

3) ERROR:KPLFLW: NO CONVERGENCE
4) ERROR:KPLFLW: RETRY ERROR
5) ERROR:KPLFLW: WRONG SOLUTION FOUND -I
6) ERROR:KPLFLW: WRONG SOLUTION FOUND -II
7) ERROR:KCOMO: NO INITIAL STRESS FOUND
8) ERROR:KCOMO: REASON INDETERMINED
9) ERROR:KCOMO: NO STRESS C. IN 1.IT
10) ERROR:KCOMO: NO CONVERGENCE
11) ERROR:KCOMO: NO VISCOUS STRESS FOUND
12) ERROR:KDASTA: VOLUME FRACTION - OLD
13) ERROR:KDASTA: VOLUME FRACTION - NEW
14) ERROR:KDEGRA: VOLUME FRACTION!
15) ERROR:KDEGRA: SYMMETRY NOT SATISFIED
16) ERROR:KDEGRA: SHAPE NOT SATISFIED
18) ERROR:KDIJPS: SYMMETRY NOT SATISFIED
19) ERROR:KDIJPS: SHAPE NOT SATISFIED
20) ERROR:KCIJPS: SYMMETRY NOT SATISFIED
21) ERROR:KCIJPS: COUPLING TERMS
24) ERROR:KTSAIH: NON-REAL FACTOR OF EXERTION
25) ERROR:KTSAIW: NEGATIVE FACTOR OF EXERTION
26) ERROR:KTMTXB: DIJNEW!=DIJOLD
29) ERROR:KTXINV: MATRIX INVERSIN FAILED
30) ERROR:UMAT: DIJ UNSYMM
31) ERROR:UMAT: DIJ ENTRIES
32) ERROR:UMAT: MODEL ERROR
33) ERROR:UMAT: PLASTICITY ERROR
34) ERROR:UMAT: NEGATIVE ENERGY
36) ERROR:UMAT: CF BENEVISTE
37) ERROR:KCOMO: NO VISCOUS CONVERGENCE
41) ERROR:KMBRAK: NO BRACKET FOUND
42) ERROR:KBRENT: MAXIMUM ITERATIONS EXCEED
43) ERROR:UMAT: PLEASE CHECK UMAT INPUT